Manuscript version: Accepted 19 February 2021
Elsevier, Materials Science & Engineering
https://doi.org/10.1016/j.msea.2021.140999

Nano-scale simulation of directional solidification in TWIP stainless steels: A focus on plastic deformation mechanisms

Mehran Bahramyan ∗, Reza Taherzadeh Mousavian, James G. Carton, Dermot Brabazon

I-Fo rm, The SF I Research Centre for Advanced Ma nufacturing, Scho ol of Me chanical & Ma nufacturing Engineering, Dublin City University, Dublin 9, Ireland

E-mail addresses: mehran.bahramyan2@mail.dcu.ie, rtaher1898@gmail.com

ABSTRACT: In this study, in order to understand the nanostructure of FeCrNi steels in the laser powder bed fusion (LPBF) process, directional solidification was simulated using large-scale molecular dynamics simulation (LSMDS). For this purpose, an atomic box with a dimension of including random dispersion of Fe, Cr and Ni was created. Then, two different fixed temperatures were considered for the left and right side of the box during cooling from the liquid molten state. For evaluation of the uniformity in mechanical properties, uniaxial tensile tests were performed in the parallel and perpendicular directions. Extensive twinning induced plasticity (TWIP) occurred alongside Shockley partial dislocations (DLs) evolution in both directions, while different ultimate tensile strengths (UTS) were obtained as a sign of non-uniform tensile behavior. Different plastic deformation mechanisms at the nano-scale including stacking faults (SFs) interaction with each other/grain boundaries (GBs)/twin boundaries (TBs), formation of defective coherent twins (DCTs), dynamic Hall-Petch, shear stress gradient (back stress), and a new mechanism for dynamic recrystallization at room temperature are discussed in detail.

Keywords: TWIP Stainless steel, Directional solidification, Plastic deformation, Molecular dynamics simulation

To cite this Publication: Mehran Bahramyan ∗, Reza Taherzadeh Mousavian, James G. Carton, Dermot Brabazon, Nano-scale simulation of directional solidification in TWIP stainless steels: A focus on plastic deformation mechanisms, https://doi.org/10.1016/j.msea.2021.140999

1. Introduction

Manuscript version: Accepted 19 February 2021
Elsevier, Materials Science & Engineering
https://doi.org/10.1016/j.msea.2021.140999

Rapid directional solidification is known as an integral part of manufacturing processes of metallic parts both in conventional casting and modern processes like additive manufacturing (AM) such as LPBF processes [1,2]. It is difficult to directly observe nano/microstructural evolution during deformation of metals and alloys. Therefore, new methods are required to study the nanostructure of additively manufactured alloys. In order to study nanostructural evolution, molecular dynamics (MD) [3] simulation can be used [4,5]. MD has gained attention in nucleation-solidification research due to its suitable length scale [6]. These simulations have been used to study solidification in a system containing thousand to millions of atoms and their accuracy is highly dependent on the used interatomic potential [7]. MD simulations of rapid directional solidification are rare, yet it is of great interest for the AM community. Recently, researchers have used MD for simulation of the AM process for the prediction of nanostructural evolution [[8], [9], [10], [11], [12], [13], [14], [15], [16], [17]]. In some of these studies directional solidification was considered and the solidified microstructures were characterised. Mahata et al. [8] considered this type of solidification for Al–Cu alloys. The effect of orientation on mechanical properties of such alloys was discussed in their study.

To the best knowledge of authors, no MD study has been reported on the basis of directional solidification in Fe–Cr–Ni SS to evaluate the solidified microstructure and uniaxial tensile behavior parallel and perpendicular to the solidification direction. However, outside of directional solidification, some other researchers have evaluated the microstructural evolution of similar metals and alloys using MD. Karewar et al. [18] studied the effect of different defect configurations and their arrangements in the FCC phase in pure iron. They considered three different defects: parallel TBs, intersecting SFs and intersecting SFs and TBs. Their results showed that parallel TBs presented the lowest barrier sites for atomic shear while intersecting SFs presented a stronger barrier for the shear stress and intersecting the SF and TB resulted in a combined effect. In a study be Zhao et al. [19], the role of deformation twinning in nanocrystalline Cu in addition to conventional DL slip has been studied using LSMDS. Based on their report the successive motion of double Shockley partials can form unstable thin twin plates. Also, the successive passage of the same twinning DLs on neighboring slip planes can form stable deformation twins along one primary twinning system or symmetric twinning systems. Jun et al. [20] studied the effect of compressive loading direction along different crystal orientations of nano-twinned Ni. Their results showed that the DLs slip toward the adjacent twin layers because they are strongly hindered by twin boundaries. Different twin boundary spacing at various temperatures have been investigated by Yan et al. [21]. Their results show that the strength of HEAs at all tested temperatures increases with decreasing twin

Manuscript version: Accepted 19 February 2021
Elsevier, Materials Science & Engineering
https://doi.org/10.1016/j.msea.2021.140999

boundary spacing until a lower critical value of 1.83 nm is reached, which is close to the experimental value (2 nm). Mohammadzadeh et al. [22] studied the effect of grain size on the nucleation sites and fraction of mechanical twins in TWIP steel. The density of nucleation sites and their developing is affected by partial DL substructure as SFs can act as a nucleation sites for the formation and thickening of twins. They concluded that by decreasing the grain size, deformation of nanocrystalline TWIP steels by mechanical twinning can be difficult due to the requirement for a higher stress for emission of Shockley partial DLs from the GBs. In another study of Mohammadzadeh et al. [23], the twin formation and detwinning processes were investigated in TWIP steel. They showed that detwinning is the reverse of the deformation twin growth via eliminating one twin layer after the layer via the reverse glide of trailing partial DLs with the same burger vector and schmid factor as the leading partial DL in the twinning process. Wang et al. [24] reported the new physical insights on the stacking fault dynamics in TWIP steels using meta-atom MD simulations. The dual role of deformation twins as both the DL barrier and DL storage has been investigated using the complex twin-slip and twin-DL interaction study.

In this study, rapid directional solidification was performed using LSMDS for FeNiCr (Fe - 13% Ni and 17.5% Cr) which is close to austenetic SS composition, by applying a temperature gradient. The polycryatalline structure was produced after directional solidification and the uniaxial tensile loading was applied in two different directions for deformation and study of the mechanical behavior of the alloy.

2. Simulation details

Embedded Atom Method potential recently developed by Zhou et al. [25] was used for describing the inter-atomic interaction between Fe–Ni–Cr using DFT. This potential is suitable for studying the mechanical properties of austenitic TWIP steel because it captures the elastic constants, stacking fault energies, cohesive energies, volume change for different compositions and more importantly, stability of random solid solution alloys at high temperatures without formation of secondary phase and solute cluster. In this study, simulation of face-centered-cubic (FCC) austenite phase of stainless steel containing Fe matrix with substitutional Ni and Cr has been performed.

Fig. 1 shows the schematic of LPBF process in which high power-density laser is used to melt and fuse the metallic powder. As the laser beam is scanned over the metallic powder, the melt pool is created and solidifies with a high cooling rate. It should be noted that the simulation of the solidification process and heat transfer in AM is too complicated and the directional solidification could be

Manuscript version: Accepted 19 February 2021
Elsevier, Materials Science & Engineering
https://doi.org/10.1016/j.msea.2021.140999

occurred in different directions. Here, due to the limitation of the MD simulations, one dimensional directional solidification was considered to understand the effect of load direction, the mechanical properties and deformation mechanisms at nano scale. In order to study this one dimensional rapid solidification process at the atomic scale in transition area, a large-scale simulation box with size of about containing 15 M atoms was created as region 1, shown in Fig. 1. In this large scale box, Fe atoms with FCC structure was created and 13% Ni and 17.5% Cr were randomly distributed. In order to bring the simulation box to the molten stage, the box was heated and equilibrated at 2700 K for 300 (ps) with a time step of 3 fs. Nose-Hoover thermostat and Parrinello-Rahman barostat were used to control the temperature and pressure, respectively. Periodic boundary conditions were applied to the all three directions for preparation of molten phase.

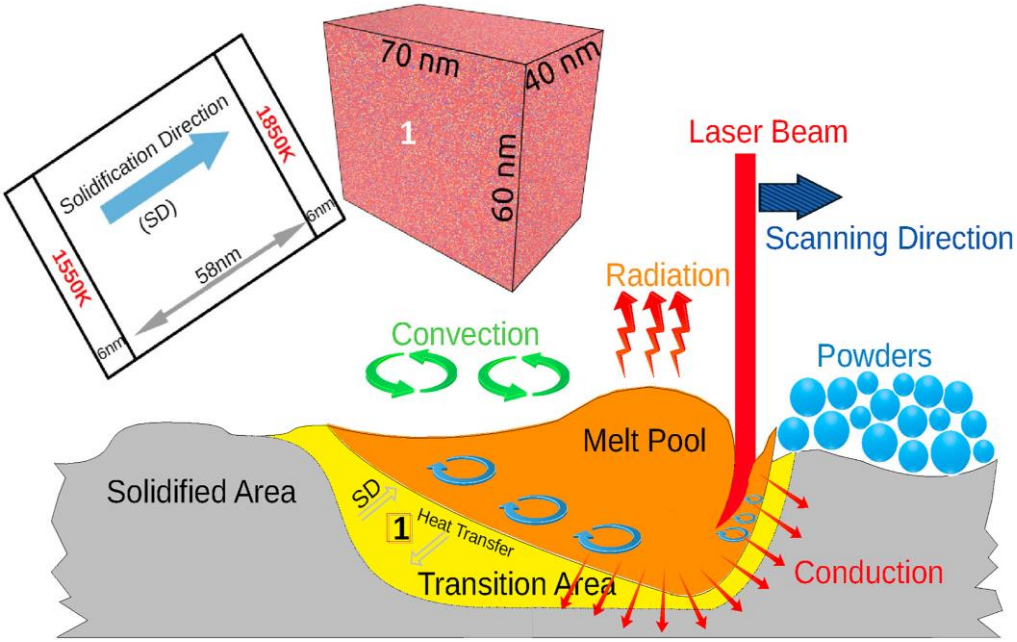

Fig. 1. Schematic of the LPBF process and location of nano size MD box for simulation of directional solidification and evaluation of the microstructure in FeCrNi TWIP steels.

To apply the directional solidification, the simulation box was divided to three regions as shown in top left subset of Fig. 1. The left side region as the low temperature region was kept at a constant temperature of 1550 K while the right region as the high temperature region was kept at a constant temperature of 1850K. These temperatures were chosen based on the phase diagram melting temperature range for SS 316 L of 1663 K–1713 K. The thickness of these two regions was 6 nm and they were kept constant using Langevin thermostat during the solidification process. The temperature for the middle region was not controlled to create the thermal gradient. During the solidification, the boundary condition for the solidification direction was set as not periodic.

Manuscript version: Accepted 19 February 2021
Elsevier, Materials Science & Engineering
https://doi.org/10.1016/j.msea.2021.140999

In order to study the mechanical properties and deformation mechanisms of the solidified structure, uniaxial tensile loads were applied with strain rate of in the solidification direction and perpendicular to the solidification direction at room temperature.

LAMMPS code [26] was used to perform all MD simulations and OVITO visualization package [27] was used to visualize the melting, solidification and deformation processes. Common Neighbor Analysis (CNA) [28,29] and Dislocation Extraction Algorithm (DXA) [30] were used to identify the local crystalline structure and perform DL analysis, respectively.

3. Results and discussion

3.1. Directional solidification

Due to the nature of the LPBF process, in which a thermal gradient is formed during heating/reheating between the tracks and layers, a directional solidification setup was created. As can be seen from Fig. 2 (a), the initial nucleus formed from the left side of the box, indicating a heterogeneous solidification based on the nature of the LPBF process. These nucleation sites act as solid seeds for the rest of the liquid to be solidified. The estimated solidification rate was around. The solidification front travels towards the liquid and gradually transform to the solid crystalline FCC structure along the temperature gradient as shown in Fig. 2(a–d) which shows the formation of austenite phase which means that a single austenitic steel was formed based on the mention chemical composition. This phase structure was already reported in literature [31,32]. Due to the high number of atoms some elongated grains and GBs were detected by continuing the solidification from left to right. In addition, as can be seen from Fig. 2(b–d), a considerable number of thermal twins and SFs in red color were detected inside the grains. The orientation of SFs and twins with respect to each other is based of (111) crystaline planes in the FCC austenitic structure. Based on Fig. 2 (e) which shows the local orientation compared with z direction, a considerable difference can be seen between the orientation of the grains and the direction of the perfect/defective twins located within these grains, contributing to GBs in Fig. 2 (d) are high angle grain boundaries (HAGBs). It can be understood from Fig. 2 (e) that TBs can divide a grain into several sub-grains with different orientations, which is why during deformation they affect the plasticity based on dynamic Hall-Petch mechanism, blocking DLs in a smaller area.

Manuscript version: Accepted 19 February 2021
Elsevier, Materials Science & Engineering
https://doi.org/10.1016/j.msea.2021.140999

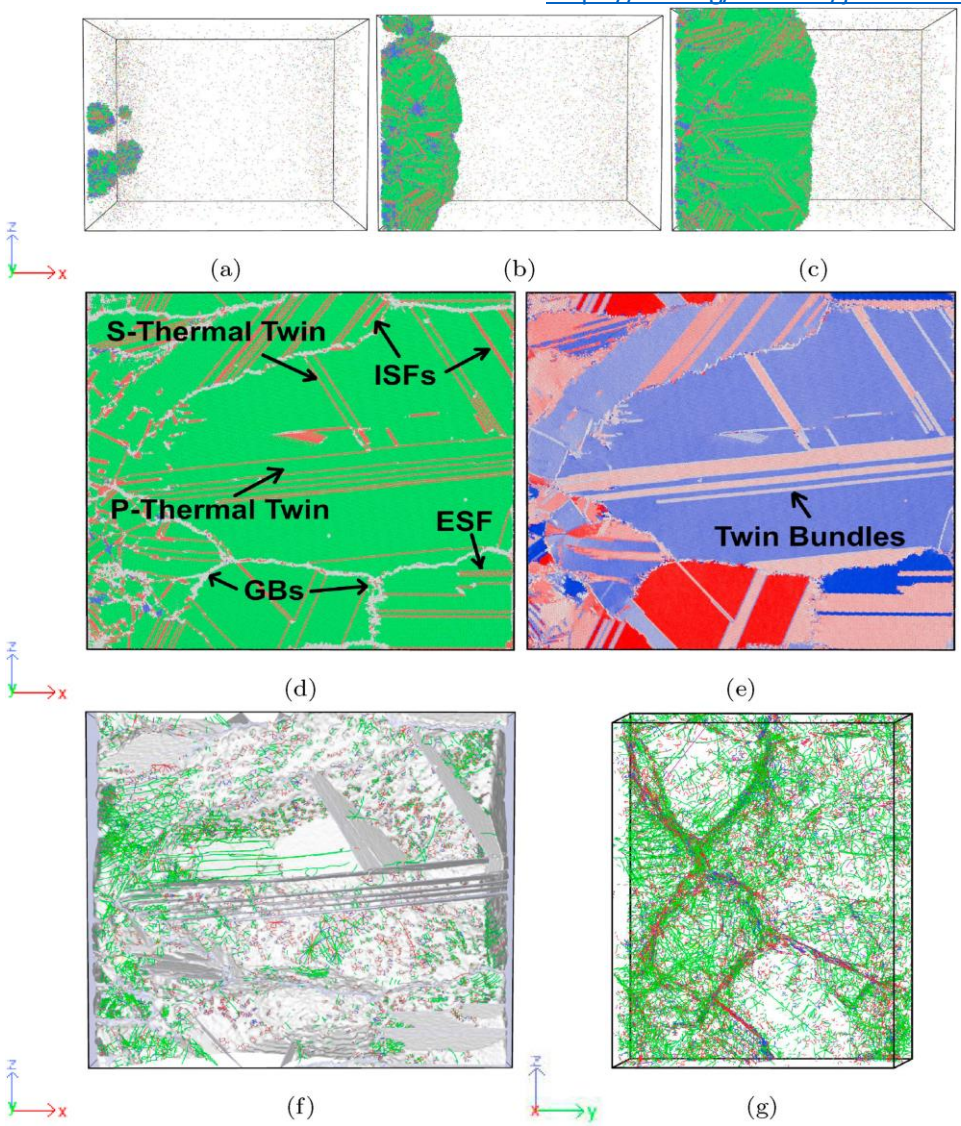

Fig. 2. Formation of crystal structure from the liquid phase during solidification after a) 150 ps b) 450 ps c) 1.5 ns d) The final solidified structure shown as region 1 in Fig. 1 containing grains with high density of defects such as thermal twins (primary, P and secondary, S), GBs and SFs (different colors show different crystal structure as green for FCC, blue for BCC, red for hcp and white for unknown crystal structure) e) Formation of grains with different orientation after solidification. f,g) Corresponding DL structure after solidification from two different viewpoints (different colors show different Burgers vector (blue color for 1/2[110] perfect, green for 1/6[112] Shockely partials, pink for 1/6[110] Stair-rod DL, yellow for 1/3[001] Hirth, Cyne for 1/3[111] Frank and the red color for unknown Burgers vectors DLs)). (For interpretation of the references to color in this figure legend, the reader is referred to the Web version of this article.)

Finally, based on Fig. 2 (f,g) a high density of DLs with different Burgers vector specially Shockley partial DLs (which can be considered as feature for TWIP steels) are detected on the left side and around the GBs after solidification. This

Manuscript version: Accepted 19 February 2021
Elsevier, Materials Science & Engineering
https://doi.org/10.1016/j.msea.2021.140999

high DL density corresponds to the rapid and non-equilibrium solidification which is an integral part of AM processes.

3.2. Tensile properties

In order to understand the difference between the tensile behavior a uniaxial tensile test was applied to the obtained polycrystalline structure along and perpendicular to the solidification direction. The stress strain response and some snapshots corresponding to the deformation stages of the samples are shown in Fig. 3. Regardless of considerable difference between the UTS values, the response trend in the plastic region in both directions was the same. Regarding the difference between UTS values, in-situ snapshots are required to understand how the loading direction can affect strain hardening which was seen to result in a higher UTS for the x direction.

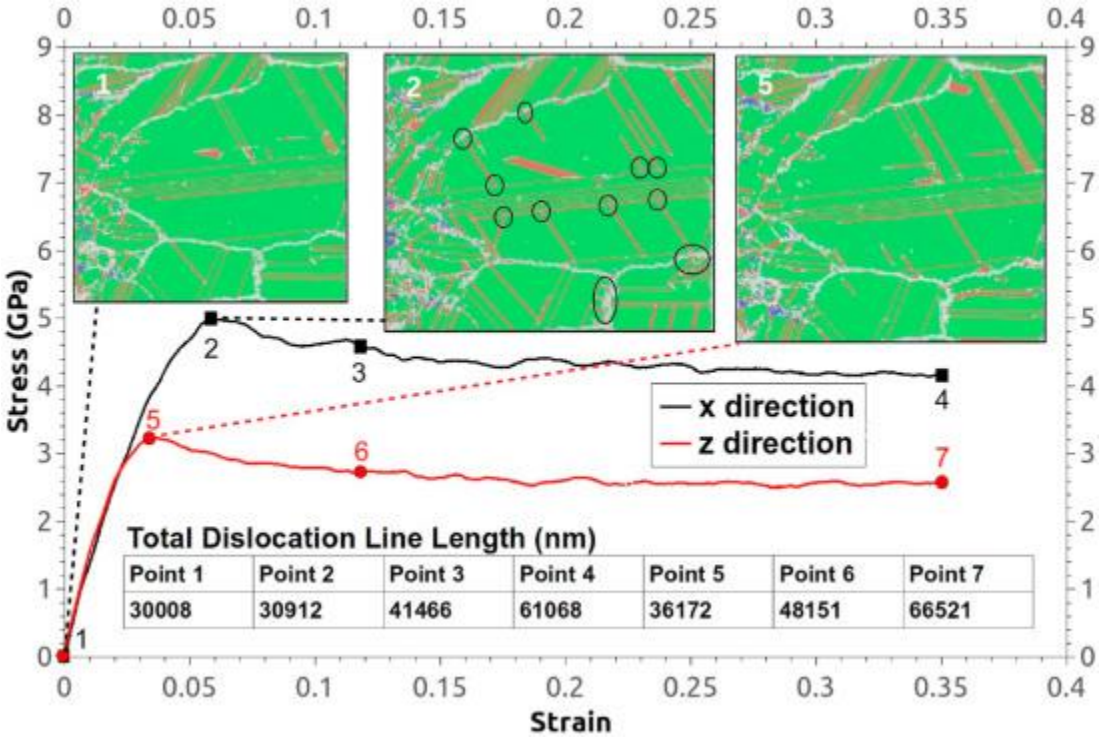

Fig. 3. Stress-strain curves of uniaxial tensile test parallel (x direction) and perpendicular (z direction) to the solidification direction at the strain rate of 10^9 (1/s). The snapshots in the picture illustrate deformation stages of the box in points 1, 2 and 5 during tensile loading. Total DL line length for all the points (1–7) are tabulated.

Based on Fig. 3, the corresponding snapshots for x and z directions at UTS points (point 2 for x and point 5 for z direction) indicated that the loading direction in TWIP alloys highly affects the activation of SFs and their interactions with single twins and GBs (black owls) during deformation. This matter has been already mentioned in the literature and it is known that Schmidt factor is responsible for

Manuscript version: Accepted 19 February 2021
Elsevier, Materials Science & Engineering
https://doi.org/10.1016/j.msea.2021.140999

activation of SFs and TBs. Although, the grains were elongated toward solidification direction (x), it seems that difference in mechanical properties after directional solidification from different orientations might not be due to GBs structure. In order to achieve a better insight between the obtained microstructures, DL density at different snapshots were estimated and the results were tabulated in Fig. 3 as DL line lengths. A higher formation of DL lines in the z direction was detected and this increasing trend was continued up to points 4 and 7. More DL fraction and activity reduced the required stress for deformation. However, in-depth in-situ microstructural characterization is required to understand the details of microstructural evolution (such as plastic deformation mechanisms and twinning/de-twinning), interaction of DLs (SFs) with each other and the formation of DL forest, as provided in the following sections.

3.3. Microstructural evolution and plastic deformation mechanisms during tensile loading

Based on the literature (experimental studies) [31,32] DL slip and TWIP mechanism are considered as the two significant mechanism for obtaining a high value of ductility in FeCrNi based stainless steels. In this study thanks to the capability of reliable LSMDS, the details of microstructure evolution was studied. Fig. 4, Fig. 5, Fig. 6 shows the phase evolution and shear strain map from different snapshots during tensile loading. In contrast with few reports [33] not too much phase transformation from austenite to martensite (Transformation-induced plasticity (TRIP)), was detected in this study as the austenite phase (green colored area) was highly stable during deformation. On the other hand, compared with Fig. 2 (d), significant interaction of DLs (SFs) with GBs, thermal and mechanical TBs occurred. Some important results were obtained from shear strain estimation in plastic region. First, the interaction of ISFs (Intrinsic Stacking Faults)/ESFs (Extrinsic Stacking Faults) with GBs and TBs caused an increment in stress/strain during deformation, making a non-uniform plastic deformation in the box. Second, it can be observed that based on the initial orientation of the grains, different slip systems were activated in this FCC structure. Based on Fig. 4 (b), the highest recorded strain is related to DL-GB interaction (points 2 and 3, see Fig. 4 (c)), ISF/ESF blockage between thermal twins and GB (point 4 and 1), defective TBs (DTBs), and multiple planar DLs slip, indicating GB(TB) and back-stress strengthening which confirms the results of Fuping et al. [34]. For strain partitioning in such TWIP steels by continuing the deformation (see Fig. 5), a higher level of shear strain was recorded. Finally, five high stress areas were detected and shown after prolonged deformation at the mentioned intersections. This significant activity of SFs between TBs and GBs has been reported [31,32] in experimental literature for such steels. Tian et al. [35] reported that partial DLs

Manuscript version: Accepted 19 February 2021
Elsevier, Materials Science & Engineering
https://doi.org/10.1016/j.msea.2021.140999

nucleated and emitted from the intersection of GB and TB, and formed new DL nucleation points by intersecting the TB. With increasing strain, the stress concentration at the intersection caused more partial DL nucleation and emission. Therefore, the high stress concentration that is shown in point 1 (see Fig. 4 (b)) can be favorable for more partial DL nucleation. Second, from Fig. 4, Fig. 5, Fig. 6, it can be understood that TBs divided all the elongated grains in two multiple sub-grains, confirming dynamic Hall-Petch mechanism. Fig. 6, indicated that there are some blue colored areas (low stress), corresponding to the lower presence and activity of DLs. In fact, it is believed that such thermal/mechanical twins can prevent the uniform activity of DLs in the microstructure. Sun et al. [36] reported that the incompatibility of deformation induced by microstructural heterogeneity (i.e. GB or TB gradient distribution) can lead to a strain gradient in TWIP alloys.

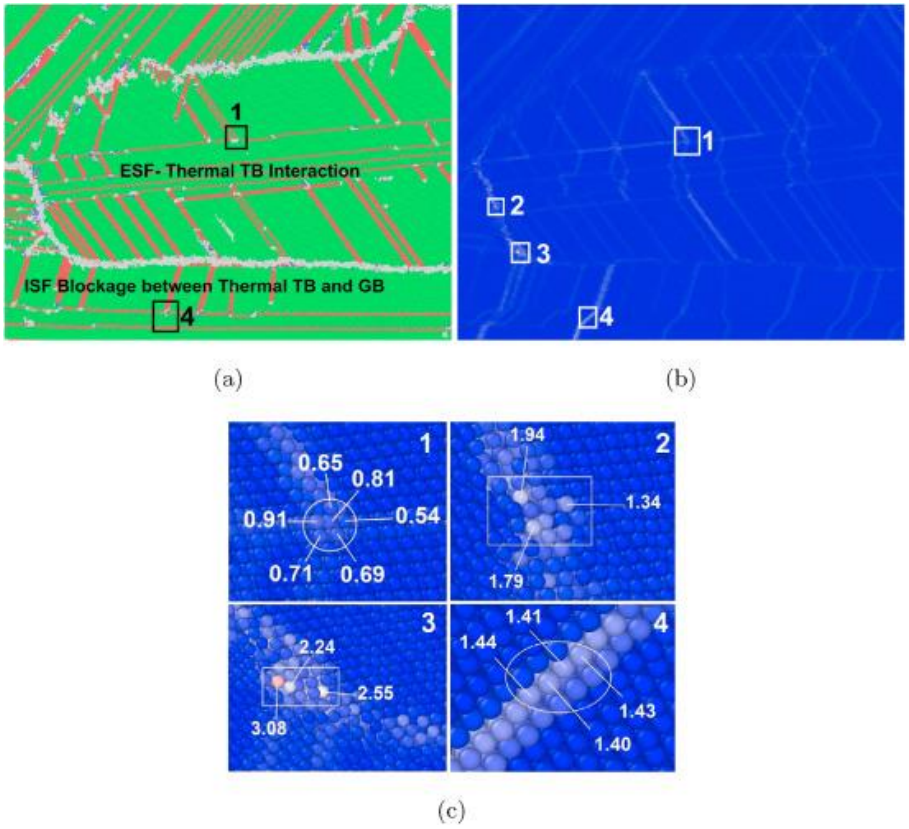

Fig. 4. a) CNA analysis and b) corresponding shear strain of the elongated grain inside the simulation box when tensile load is applied in the x direction at a strain of 9%. c) The value of the shear strain at the points depicted in (b). Blue color shows the lower value of the shear strain which is zero. (For interpretation of the references to color in this figure legend, the reader is referred to the Web version of this article.)

Manuscript version: Accepted 19 February 2021
Elsevier, Materials Science & Engineering
https://doi.org/10.1016/j.msea.2021.140999

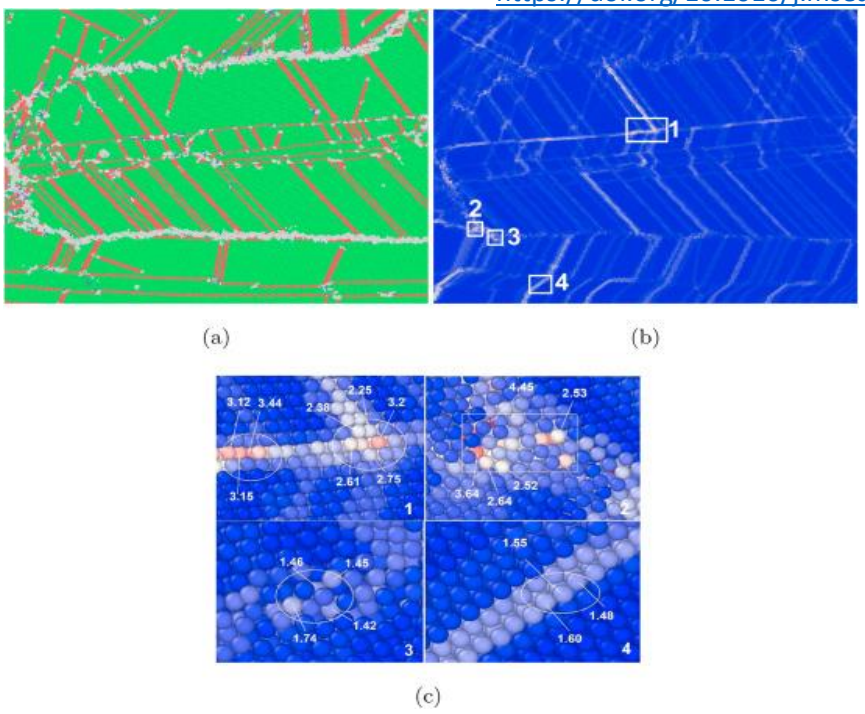

Fig. 5. a) CNA analysis and b) corresponding shear strain of the elongated grain inside the simulation box when tensile load is applied in the x direction at a strain of 21%. c) The value of the shear strain at the points depicted in (b). Blue color shows the lower value of the shear strain which is zero. (For interpretation of the references to color in this figure legend, the reader is referred to the Web version of this article.)

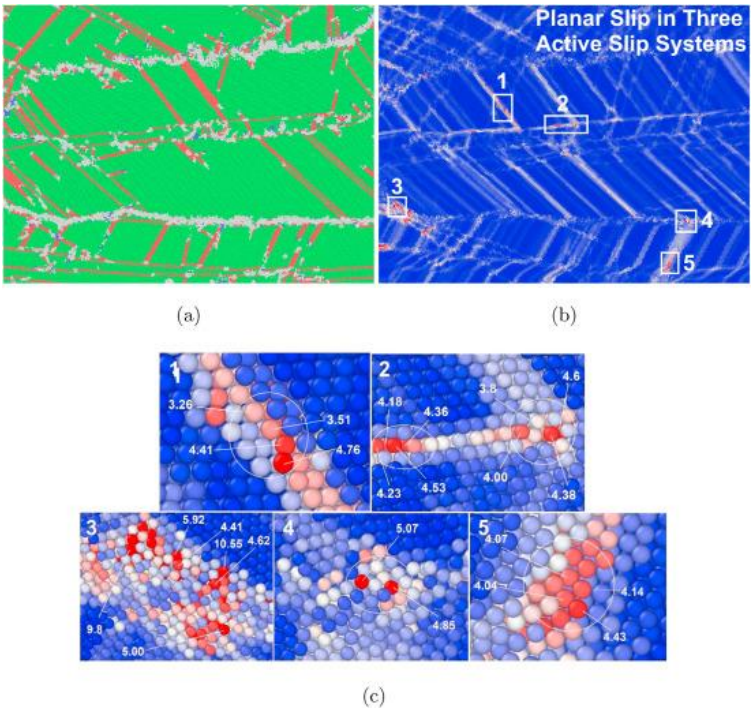

Fig. 6. a) CNA analysis and b) corresponding shear strain of the elongated grain inside the simulation box when tensile load is applied in the x direction at a strain

Manuscript version: Accepted 19 February 2021
Elsevier, Materials Science & Engineering
https://doi.org/10.1016/j.msea.2021.140999

of 39%. c) The value of the shear strain at the points depicted in (b). Blue color shows the lower value of the shear strain which is zero. (For interpretation of the references to color in this figure legend, the reader is referred to the Web version of this article.)

In order to further understand the nanostructural evolution, high-magnification microstructural characterization was performed in some areas. Fig. 7, Fig. 8, Fig. 9, Fig. 10, Fig. 11 show the gradual collision of two ISFs from two different slip systems at an area limited by a primary thermal twin (bottom side), a secondary mechanical twin (right side), and a GB (top side). Fig. 7 (a), shows a DTB having an intersection with a secondary mechanical twin (70° angle). Fig. 7 (b) presents the shear strain map. An ISF-TB parallel interaction can be observed on the right side, resulting in an increase in the stress similar to that caused by DTB and the other ISFs. It has been reported when TBs are smaller than a critical value, the partial DLs in grains slip parallel to the TB [35].

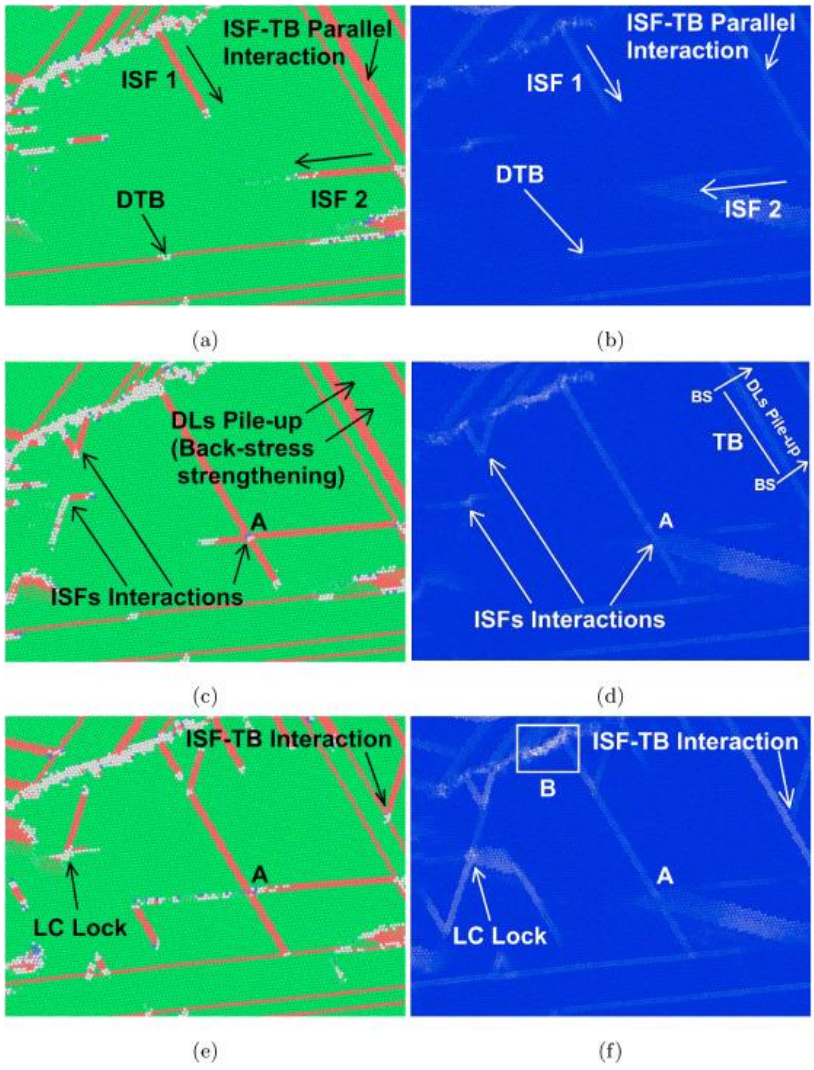

Fig. 7. CNA and corresponding shear strain analysis when tensile load is applied in the z direction at a strain of a,b) 3.43%, ISFs interactions led to the formation

Manuscript version: Accepted 19 February 2021
Elsevier, Materials Science & Engineering
https://doi.org/10.1016/j.msea.2021.140999

of DTB. Twin boundary strengthening results from parallel interaction of ISF and TB. c,d) 3.88%, Higher shear strain in the interaction area of ISFs with GBs and e,f) 4.47%, formation of LC lock in the interaction of ISFs.

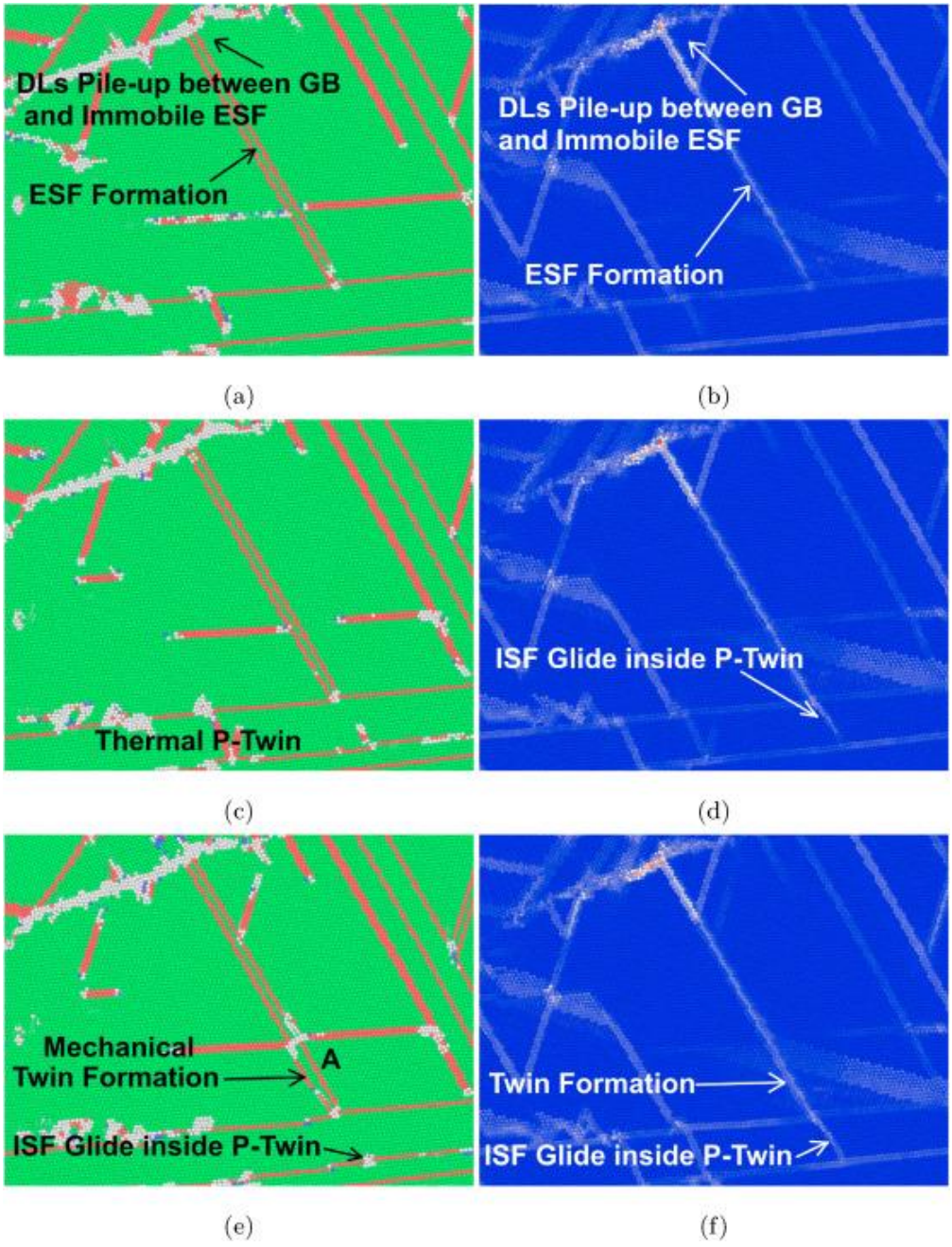

Fig. 8. CNA and corresponding shear strain analysis when tensile load is applied in the z direction at a strain of a,b) 5.37%, ISFs interactions caused ESF formation and led to DL pile-up in the ESF-GB interaction area c,d) 5.67%, Twin-mediated slip result in strain inside thermal primary twin during glide and e,f) 5.97%, nucleation of secondary twin from the DLs-ESF interaction close to the primary twin.

Manuscript version: Accepted 19 February 2021
Elsevier, Materials Science & Engineering
https://doi.org/10.1016/j.msea.2021.140999

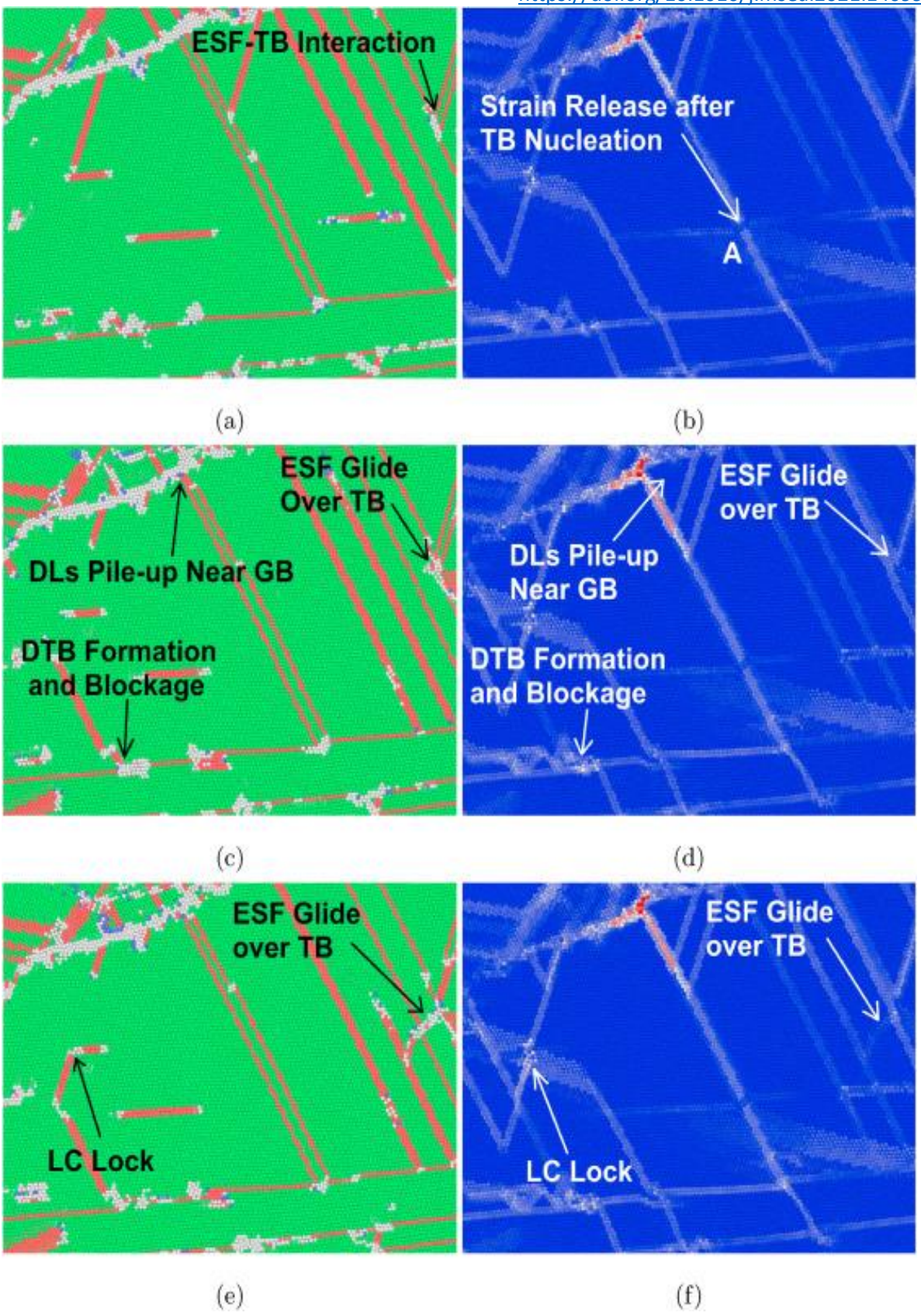

Fig. 9. CNA and corresponding shear strain analysis when tensile load is applied in the z direction at a strain of a,b) 6.41%, strain release due to the passage of DL from TB, c,d) 7.46%, kink-like step formation due to the ISFs

Manuscript version: Accepted 19 February 2021
Elsevier, Materials Science & Engineering
https://doi.org/10.1016/j.msea.2021.140999

interactions with TBs and their blockage and e,f) 7.76%, ESF-TB interaction and passing over with the same glide direction.

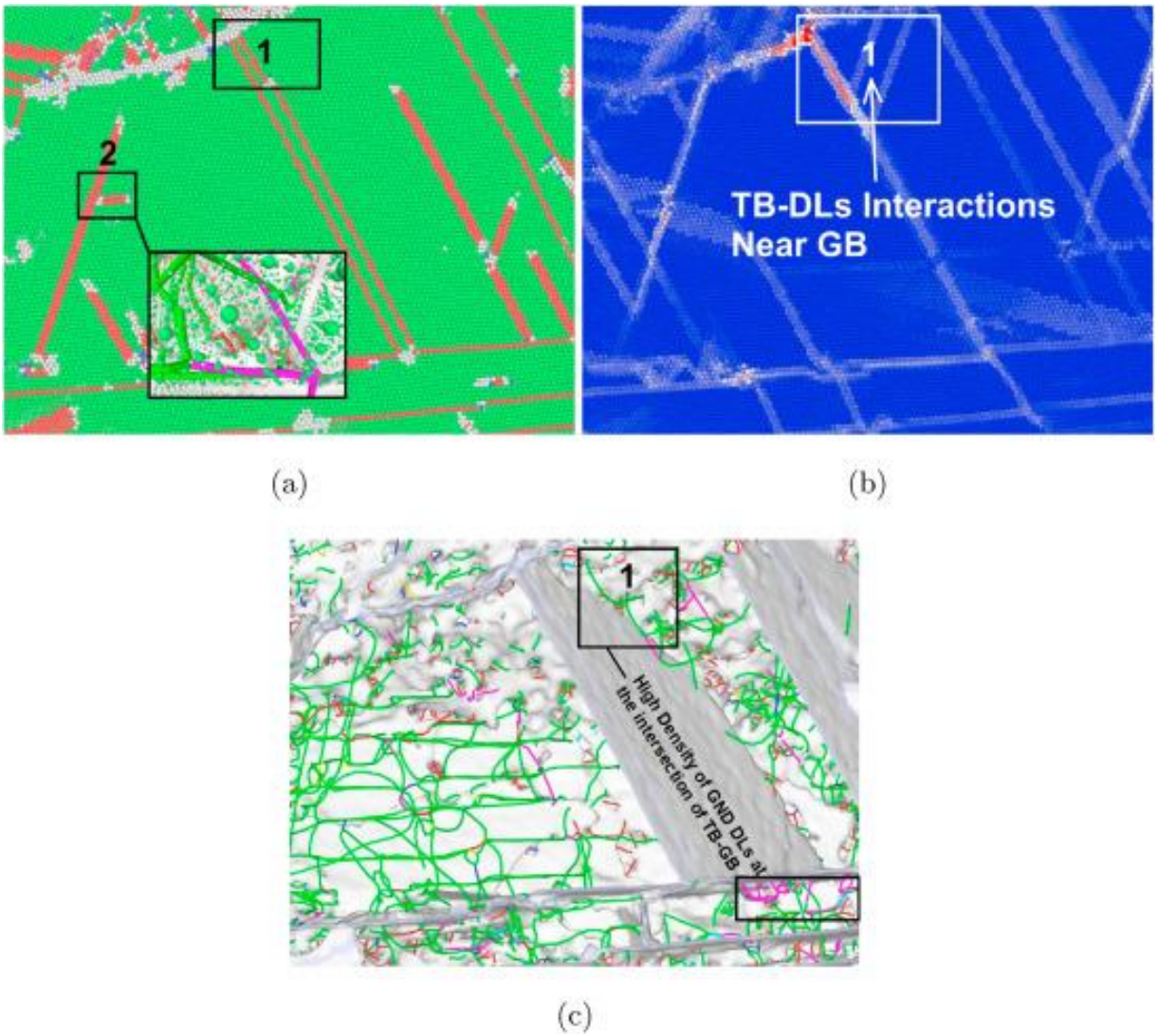

Fig. 10. a) CNA analysis, b) corresponding shear strain analysis and c) DXA analysis which show TB-DLs interactions close to the GB which result in the high shear strain in the region 1 at a strain of 8.35% when tensile load is applied in the z direction. Region 2 shows the LC lock and corresponding DL blockage.

Manuscript version: Accepted 19 February 2021
Elsevier, Materials Science & Engineering
https://doi.org/10.1016/j.msea.2021.140999

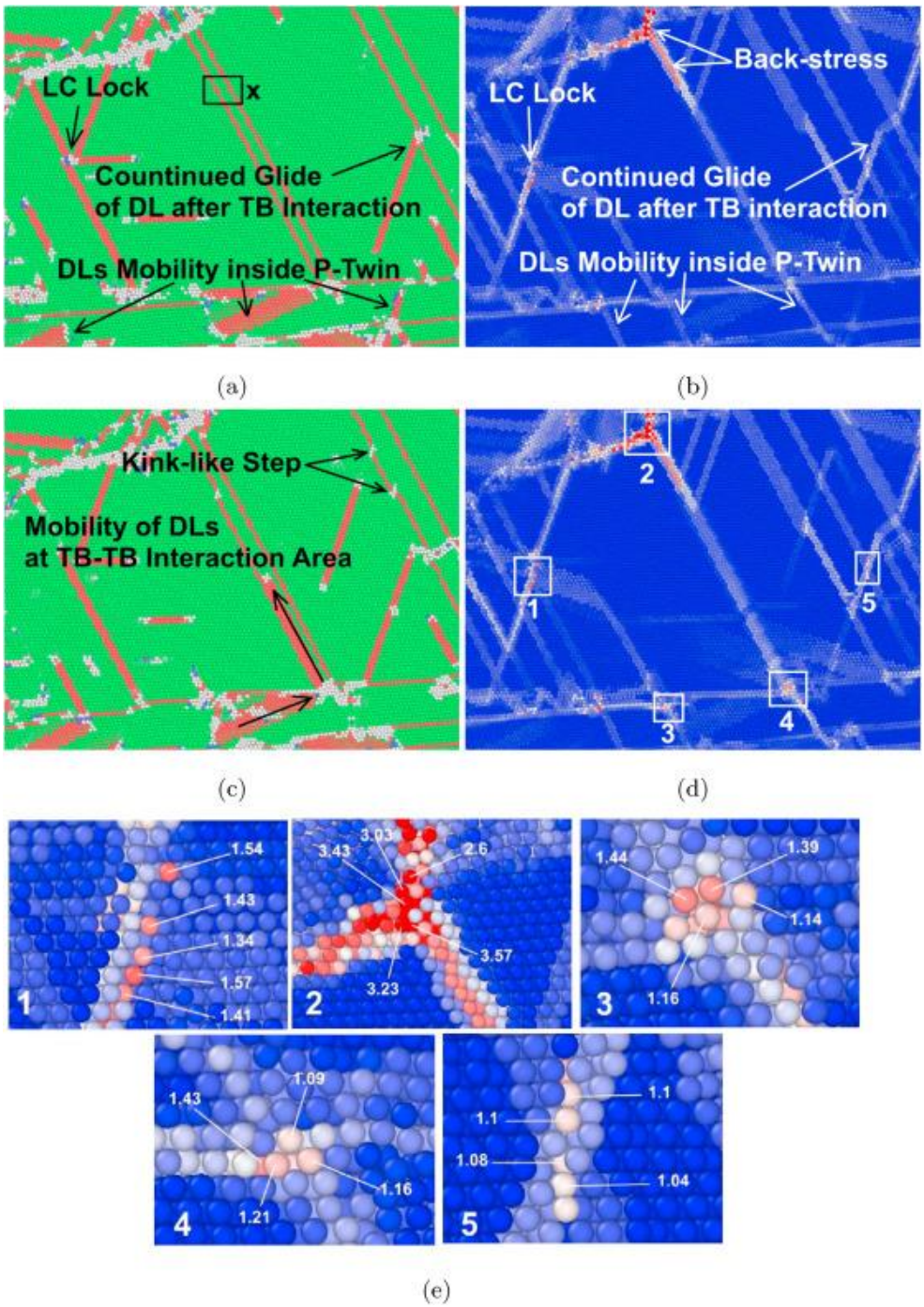

Fig. 11. CNA and corresponding shear strain analysis when tensile load was applied in the z direction at a strain of a,b) 9.55%, back stress strengthening and DL activity inside P-twin. LC lock caused an increase in the shear strain, c,d) 10.44% DLs movement from primary twin to the secondary twin which result in the strain in the interaction area. Formation of the kink-like step, and e) the value

Manuscript version: Accepted 19 February 2021
Elsevier, Materials Science & Engineering
https://doi.org/10.1016/j.msea.2021.140999

of shear strain in the regions depicted in (d). Blue color shows the lower value of the shear strain which is zero. (For interpretation of the references to color in this figure legend, the reader is referred to the Web version of this article.)

By continuing deformation three ISFs from three different slip systems had an intersection at point A. In addition, DL pile-up behind the mechanical secondary TB which caused back stress strengthening (see Fig. 7 (c) and (d)). Further deformation (7 (e) and (f)) made Lomer-Cottrell (LC) lock at the left side of the box with the high record level of stress. On the other hand, interaction of DLs from the upper and lower grains at region B increased the stress at the GB. From the right side of the box, an ISF interaction with the secondary mechanical TB can be observed as well.

Further deformation caused the nucleation of an immobile ESF as shown in Fig. 8 (a). A triangle intersected area was then formed between GB, ISF and immobile ESF (see Fig. 8 (b)). The glide of partial DLs inside the thermal P-twin was observed and is shown in Fig. 8 (c) and (d), indicating that considerable DL slip occurs in such micro twins. Finally, a new mechanical twin parallel to the right side twin was nucleated by change of slip plane for partial DL at point A (see Fig. 8 (e,f)). Zhang et al. [37] reported that at high stress when there is limited GB activity, we have TB nucleation by DLs gliding.

From Fig. 9 (a) and (b), the growth of new TB can be observed and by glide of DLs strain release occurred at point A. Fig. 9 (c) and (d) indicated the formation of a high level of strain at the intersection of an ISF with DTB which is caused by the blockage of DLs behind DTB. Another DL glide was observed at the right side of the box from the mechanical TB by further deformation.

In addition, a high level of strain was recorded around the LC lock. In order to confirm the shear strain map result, DL structure was provided after further deformation and the results were shown in Fig. 10. Based on the literature [38,39], stair-rod DLs are formed at the LC lock and Fig. 10 (a) indicated the presence of stair-rod partial DLs (pink color). On the other hand, a high density of GND (Geometrically Necessary Dislocations) can be seen at region 1, at the intersection of new TB with GB that caused a high level of recorded strain (see Fig. 10 (b)). Zhi et al. [40] reported that the back stress is believed to originate from pile-ups of GNDs against barriers, rather than from the randomly distributed statistically stored dislocations (SSDs) in materials. At the bottom of Fig. 10 (c) severe formation and interaction of stair-rod DLs (pink color) was detected, indicating that glide of Shockley partial DLs across the TBs is not always occurring during microstructural evolution of such TWIP steels which can be

Manuscript version: Accepted 19 February 2021
Elsevier, Materials Science & Engineering
https://doi.org/10.1016/j.msea.2021.140999

considered as strengthening mechanisms similar to LC locks and DLs pile-up at region 1.

Fig. 11 (a) and (b) showed the full formation of new mechanical TB between primary TB and GB. In addition, significant mobility of DLs can be observed in a new slip system inside P-twin. From Fig. 11 (c) and (d), transition of DLs from PTB to new formed mechanical twin which caused a high level of strain at the intersection can be observed. It should be noted that the glide of DL along the new formed TB which is shown by a black colored array in Fig. 11 (c) is considered as a softening mechanism [41]. Also, kink-like steps were formed due to DLs interactions with TB as reported in literature [42,43]. Comparing the corresponding shear strains at five different regions (Fig. 11 (e)) indicated that DLs were tangled at the intersection of new formed TB with GB which highly increased the strain at this area with respect to the other regions.

Manuscript version: Accepted 19 February 2021
Elsevier, Materials Science & Engineering
https://doi.org/10.1016/j.msea.2021.140999

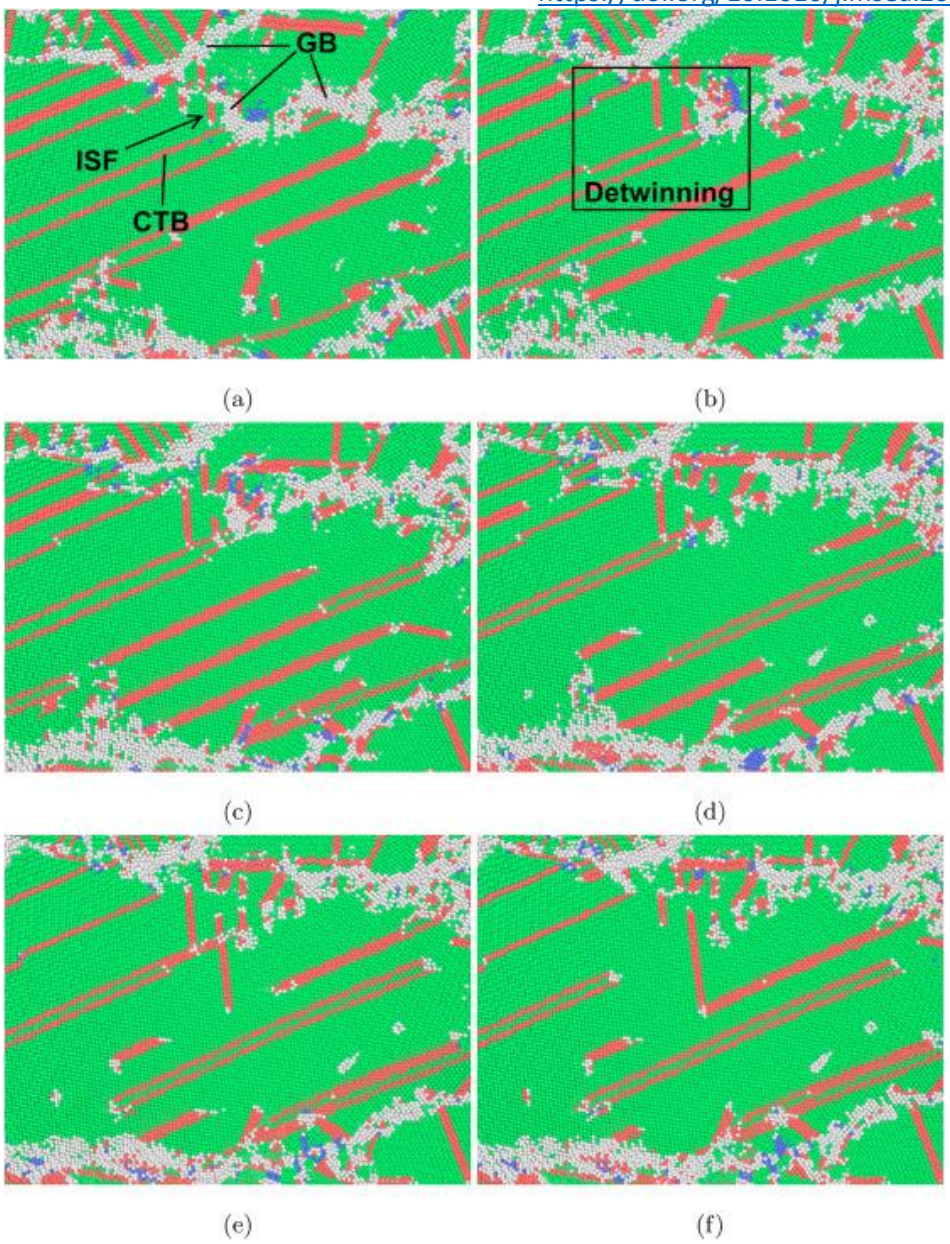

Fig. 12. Detwinning process as result of SF-Twin interaction at strains of a) 29.10%, b) 30.89%, c) 32.23%, d) 33.73%, e) 34.92%, and f) 35.07% when tensile load was applied in the z direction.

An interesting analysis from another area showed the detwinning mechanism for these TWIP steels due to interaction of an ISF with a coherent twin boundary (CTB) which is shown in Fig. 12. In this mechanism interaction of ISF changed the slip plane of twinning partial DLs and gradually full detwinning occurred. This mechanism is known as a softening process, leading to the high level of plasticity in such steels. A well-known mechanism for this detwinning process has been reported in the literature [44,45] in FCC metals. In this mechanism partial twinning dislocation (PTD) will change their slip plane and defective twin boundaries (DTBs) will form by the formation of coherent and incoherent twin

Manuscript version: Accepted 19 February 2021
Elsevier, Materials Science & Engineering
https://doi.org/10.1016/j.msea.2021.140999

boundaries (CTBs and ITBs). However, according to Liang et al. study [46], ITBs may contribute more to work hardening than CTBs, in this study no ITB was detected during the deformation.

Based on the literature [47], a higher level of stress is required for the formation of ternary mechanical nano-twins inside the secondary twins. This high stress normally occurs in alloys with a low level of SFE. It is known that reducing the SFE will change the TWIP mechanism to the TRIP mechanism during deformation. In some scientific reports the simultaneous occurrence of TWIP and TRIP has been reported in particular for high entropy alloys and high/medium manganese steels. In the current study, as shown in Fig. 13 a ternary nano-twin was detected inside a micro twin from the intersection of an ISF with DTB. Zhao et al. [48] already reported that slip-twin interactions can promote the formation of twin nuclei. This process occurs during deformation in the z direction and it is interesting that BCC phase (purple color) which might correspond to martensite was locally detected at the TB-GB intersection. This matter indicates that the required stress for the formation of ternary nano-twins and TRIP mechanism was available in that part of the box along the z direction.

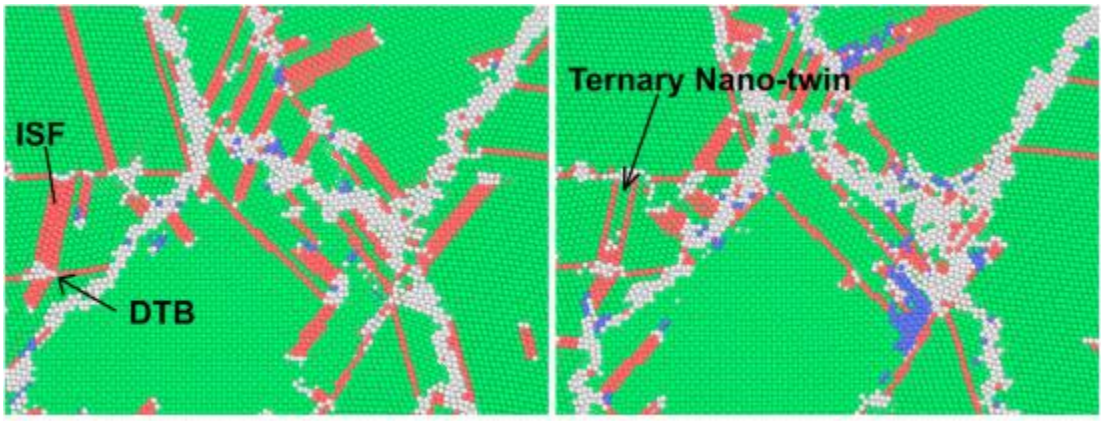

Fig. 13. Nano-twin formation inside twin at a strain of a) 15.75%, b) 26.25% when tensile load applied in z direction.

3.4. DL evolution in detail

In order to understand the evolution of DLs, and their interactions with TBs and each other (in TB-free zones), further characterizations were done. Fig. 14 shows the DXA analysis of a selected area having the motion and interaction of secondary TBs with a primary annealing twins during deformation, and revealing the nature of DLs in this area. Some points can be understood from Fig. 14. First, the fraction of green colored partial DLs (Shockley) is considerably higher than that of other types. This matter is in agreement in FCC structures when the SFE

Manuscript version: Accepted 19 February 2021
Elsevier, Materials Science & Engineering
https://doi.org/10.1016/j.msea.2021.140999
is low, meaning that the dissociation of full DLs is thermodynamically favorable. An interesting point is that the continued glide of Shockley DLs by intersections with TBs which can be considered as a softening mechanisms in such TWIP steels. Second, stair-rod DLs (pink colors) were detected and shown by black colored rectangles at the intersection of TBs. It is known that such type of DLs are not mobile enough and continued deformation from Fig. 14(a) and 14(b) indicated the sessile nature of such DLs. Third, as it can be seen from Fig. 14 (b) a high density of DLs are trapped between the primary and secondary TBs, indicating dynamic Hall-Petch mechanism as shown in the schematic. It is generally accepted that deformation twins, as planar obstacles, increase the total DL density, and thereby increase DL hardening, which refers to the so-called dynamic Hall-Petch effect. Such areas including DL nodes (huge DL interaction) were also observed in Fig. 15 including twin-free regions beside HAGB. From our deep microstructural characterization we found that intensive DLs tangle were more observed in TB-free zones, however, as shown in Fig. 14, considerable DL tangle can be formed where there are intersections between primary and secondary TBs. It should be noted that low DL activity can be detected between primary or secondary parallel TBs (TB bundles) as shown in Fig. 15 (c,d). It has been reported that smaller TBs limited the movement of DLs intersecting the TB. Such DLs required higher external pressure to cross the TB. In fact, when TBs was smaller than the critical value, the average flow stress decreased with decreasing TBs, showing an inverse Hall-Petch relationship [35]. Such hot spots of GND DL tangles that are mostly observed near the GBs (see Fig. 15 (a,b)) are considered as strengthening mechanisms by accommodation of strain gradients [49]. After LPBF of such stainless steels, due to the presence of Mo element in the chemical composition, the cellular structure including high density of DL tangle form the cell walls. The formation of such cells has been reported [31,32] as a barrier for DL movement and TB migration. In our atomic box, due to the lack of suitable interatomic potential for Mo with other elements, no cellular structure was detected after directional solidification. The type of such DL tangles in the current study is therefore different from those that have been reported around cell walls in LPBF processed stainless steel. In summary, due to the extensive effect of twinning/detwinning on ductility and strength (energy absorption) of TWIP steels, based on Fig. 6, Fig. 11 and 14(b), a suitable combination of elongation and strength can be expected by maximizing the formation of secondary mechanical twins and their interaction with primary twins and GBs. This means that the formation of intensive DL tangles such as shown in Fig. 11(b) might not be interesting for the simultaneous improvement of ductility and strength to break their trade-off. It is believed that tuning the

Manuscript version: Accepted 19 February 2021
Elsevier, Materials Science & Engineering
https://doi.org/10.1016/j.msea.2021.140999

chemical composition and SFE will highly affect the formation of secondary mechanical twins.

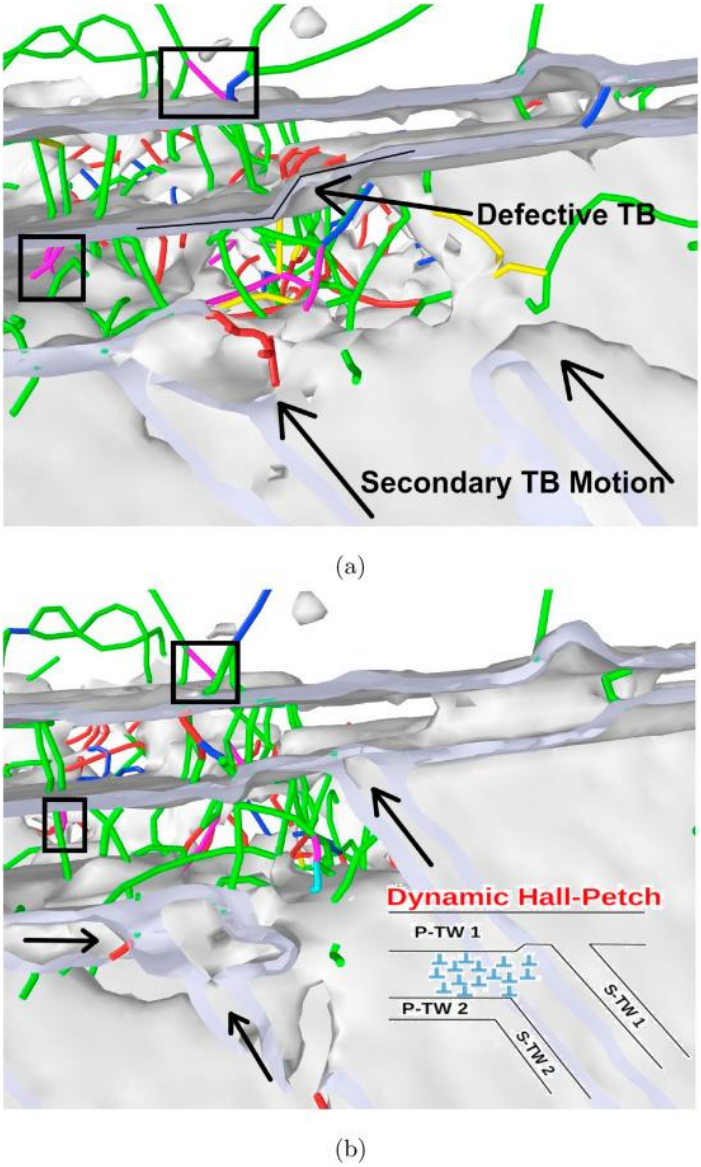

Fig. 14. Secondary mechanical twin interaction with DTB when the tensile load is applied in the x direction at a strain of a) 32.53% and b) 33.73% which shows dynamic Hall-Petch. Stair-rod DLs interactions with thermal twin, formation of defective P-twin. Shockley DLs passed over the TBs without changing their character.

Manuscript version: Accepted 19 February 2021
Elsevier, Materials Science & Engineering
https://doi.org/10.1016/j.msea.2021.140999

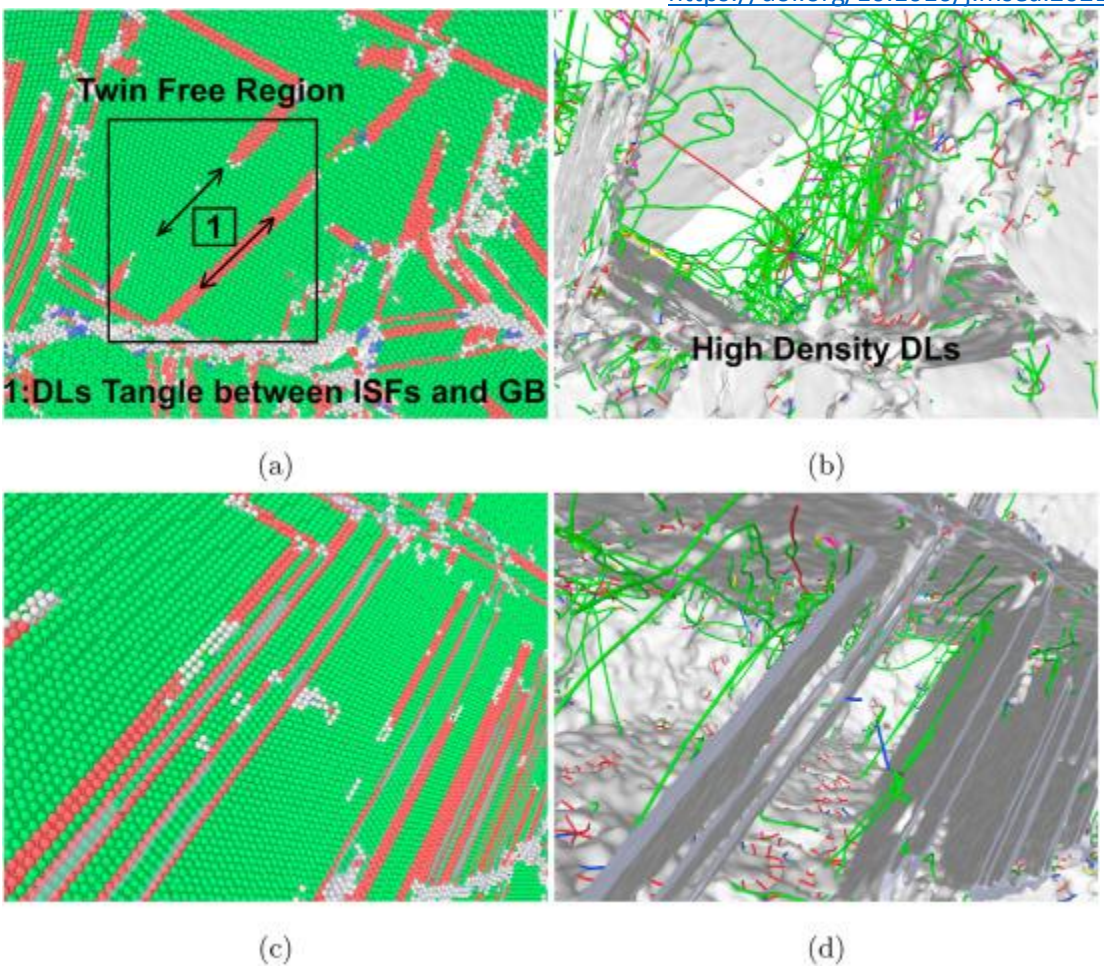

Fig. 15. a-b) High density of DLs in the twin free region at the strain of 15% when tensile load is applied in the x direction. c,d) Low DLs activities in small TBs which shows inverse dynamic Hall-Petch.

Finally, in order to elucidate DLs interactions with secondary TBs, point x from Fig. 11 (a) was selected for DXA analysis. In Fig. 16 (a,b) the collision of DLs from two different slip systems with the new formed TBs is shown. A stair-rod edge DL with Burgers vector of 1/6[110] was shown in Fig. 16 (a) and it seems that its nature was kept after interaction and also a similar behavior was detected in Fig. 16 (b) for a screw Shockley partial DL with Burgers vector of 1/6[11–2] in another slip system. It is interesting that after these interactions an immobile Frank DL with Burgers vector of 1/3[111] with an edge type was formed inside the TBs [50]. Such interactions can be considered for simultaneous improvement of ductility and strength.

Manuscript version: Accepted 19 February 2021
Elsevier, Materials Science & Engineering
https://doi.org/10.1016/j.msea.2021.140999

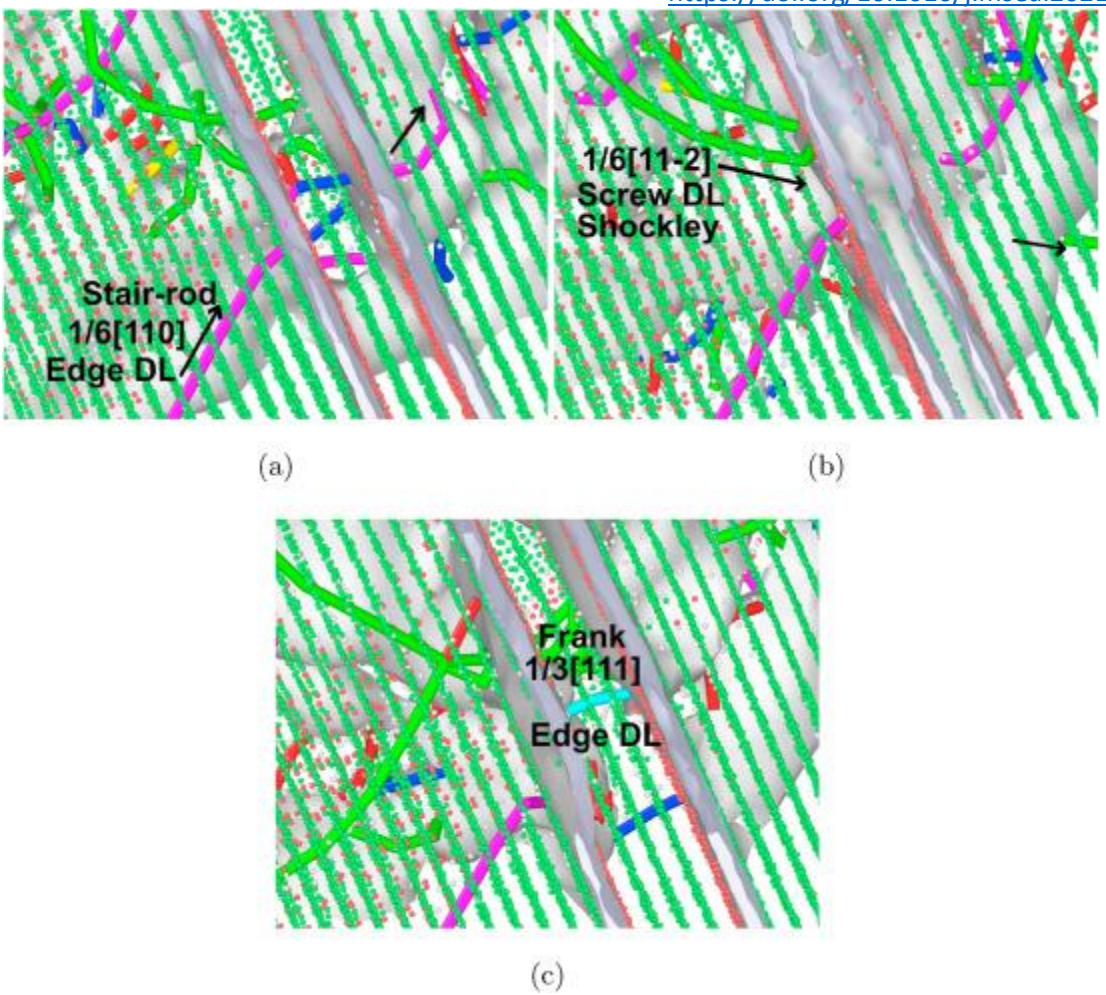

Fig. 16. Interaction of stair-rod DLs with secondary mechanical TB which led to the formation of immobile Frank DLs at a strain of a) 9.55%, b) 10.14%, and c) 10.44% when tensile load is applied in the z direction.

3.5. GBs evolution

The last part of the current study is related to evolution of GBs in such alloys. Two types of interesting evolution were detected toward loading directions x and z.

3.5.1. Migration of GBs and formation of a new grain

In Fig. 17 (a), the interaction of a TB with triple GB (black colored rectangle) is shown. By continuing deformation in the z direction, a gradual migration of GB at this area to the right side can be observed (Fig. 17(b)), making a grain with an almost round shape (see Fig. 17 (c)). It is interesting to note that a new TB was formed due to GB migration as shown in Fig. 17(b) (black colored rectangle). Zhang et al. [51] reported that deformed GBs have a great influence on the generation of twinning. Further deformation caused more interaction of SFs and TBs with HAGBs, resulting in the formation of a large grain by the gradual

Manuscript version: Accepted 19 February 2021
Elsevier, Materials Science & Engineering
https://doi.org/10.1016/j.msea.2021.140999

disapperence of GB (Fig. 17 (d)) in the middle of the large grain. Such GB migration might be considered as a softening mechanism due to the lower interaction of SFs and TBs with GBs and each other. This grain movement has been also observed in experimental work of SS 316l [52].

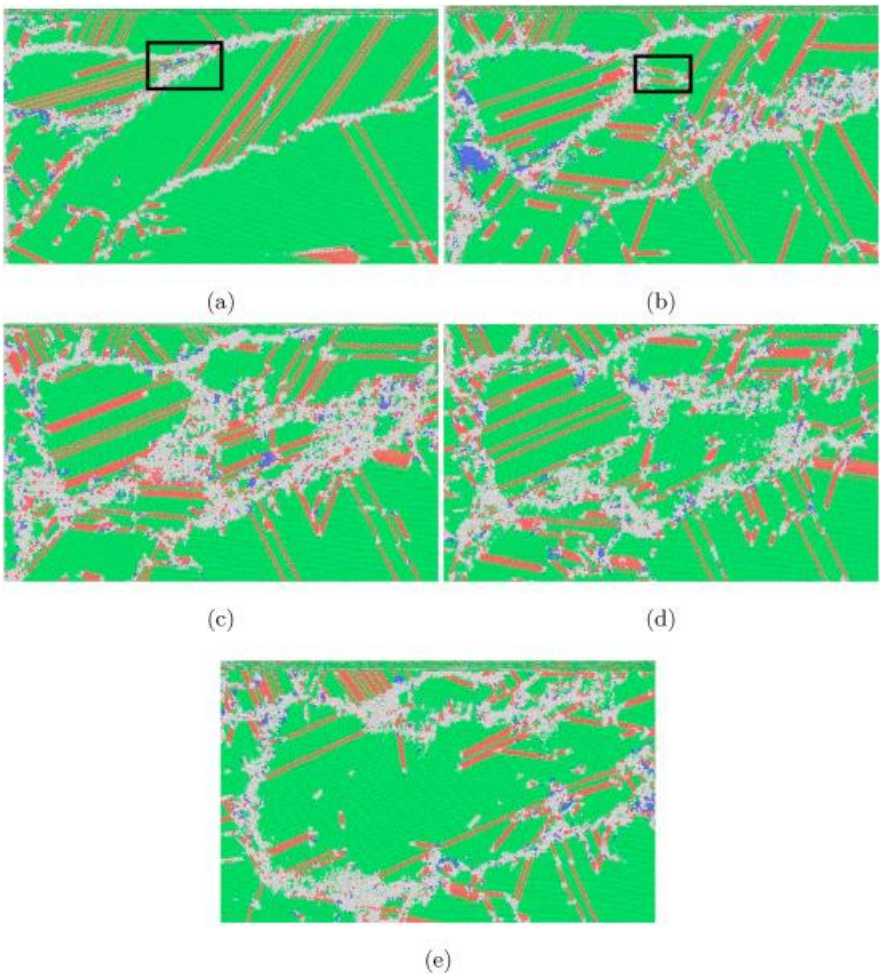

Fig. 17. TBs, ISFs and Triple GB interactions which caused GB migration process in top-left of the simulation box when tensile loading was applied in the z direction at a strain of a) 0%, b) 10%, c) 19.4%, d) 25.37%, and e) 40%.

3.5.2. Dynamic crystallization at the interaction of CTB and a triple GB

During in-situ microstructural characterization in the direction, an interesting phenomena was observed. As it can be seen from Fig. 18 (a) a conjunction between a CTB with two GBs having intersection with each other to make a triple GB made a walled area with a different crystal orientation in between. At the start of the tensile induced deformation, a gradual interaction of SFs and secondary mechanical TBs with CTB can be observed making a high stress area at the intersecting points. On the other hand, the level of shear strain at the triple GB increased successively. Intensive collision of SFs with the CTB caused a gradual appearance of white color areas with unknown coordination structure around the

Manuscript version: Accepted 19 February 2021
Elsevier, Materials Science & Engineering
https://doi.org/10.1016/j.msea.2021.140999

CTB, making a new grain surrounded by a new GB. It is interesting that the level of shear strain inside this new grain is considerably lower than the other areas (see Fig. 18 b-f). In order to further characterize this new grain, DXA and CNA analyses were conducted using a higher magnification and the corresponding results are shown in Fig. 19. Literature [53] already reported that dynamic recrystallization for LPBF produced stainless steel can occur during deformation at room temperature which can be considered as a softening mechanism for such TWIP steels. It is believed that a high density of partial DLs (SFs) formed by the high cooling rate of LPBF process and their activation around GBs can be considered as the root cause of this phenomenon for such alloys.

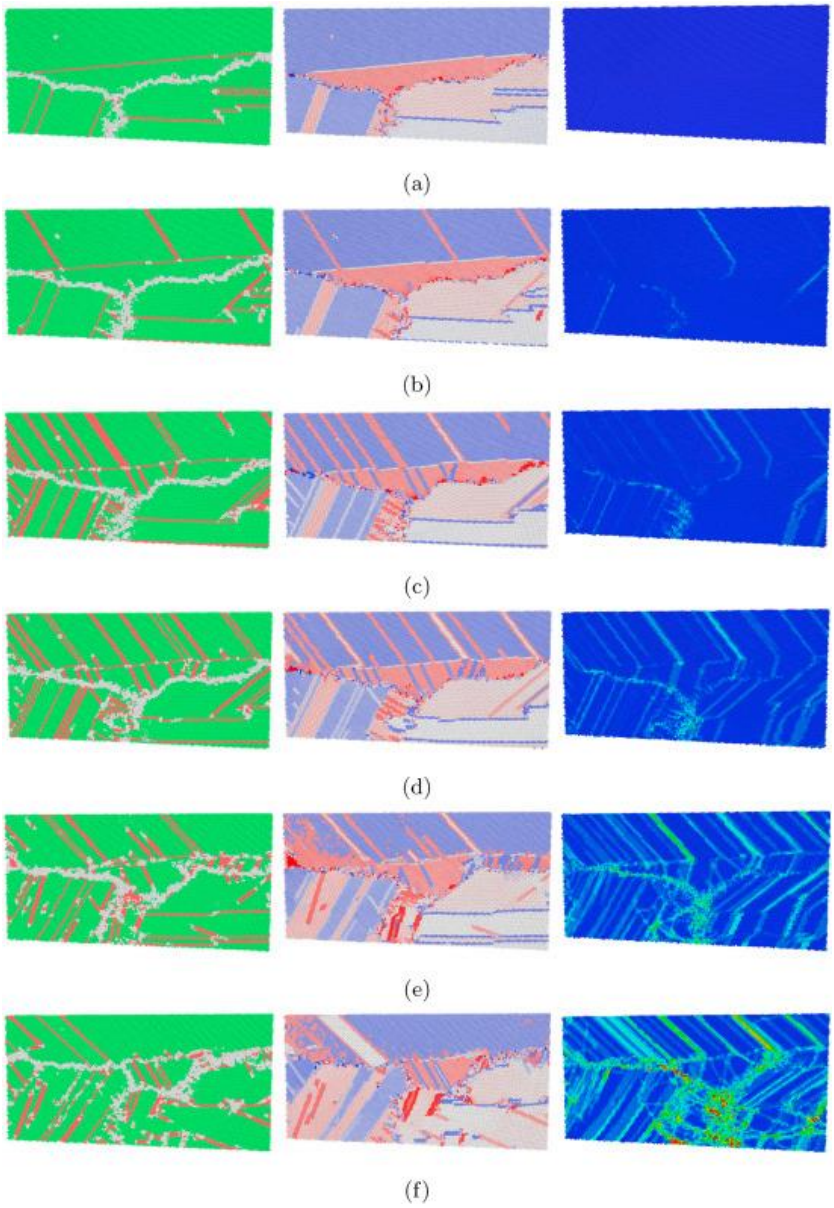

Fig. 18. CNA, orientation and shear strain results of the region where dynamic recrystallization process happened due to the interaction of CTB and triple GB

Manuscript version: Accepted 19 February 2021
Elsevier, Materials Science & Engineering
https://doi.org/10.1016/j.msea.2021.140999

at a strain of a) 0%, b) 6%, c) 9%, d) 13.5%, e) 24%, and f) 37.5% when tensile loading is applied in the x direction.

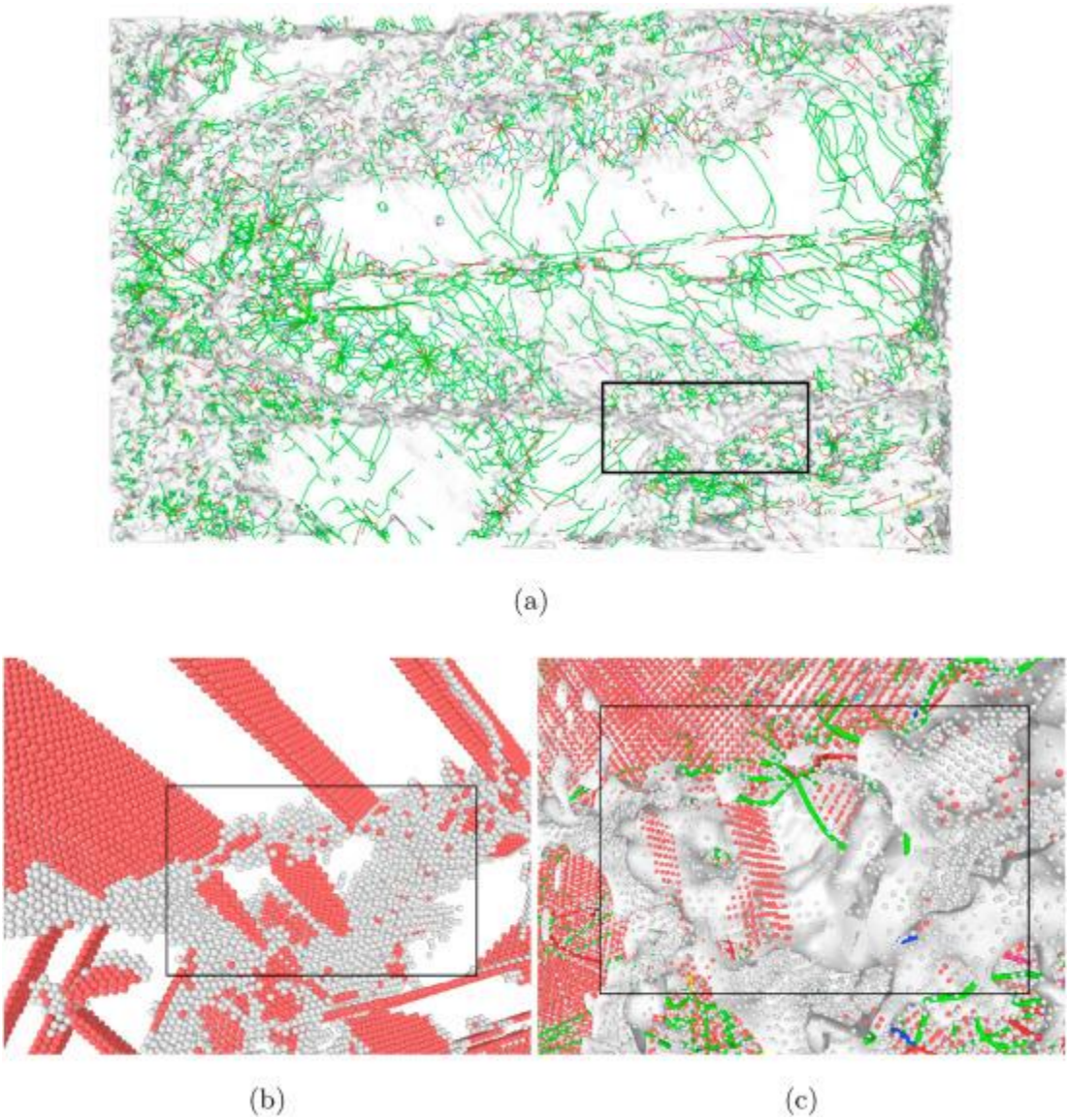

Fig. 19. a) DL structure, b) SFs and GBs, and c) SFs and GBs with DLs and defect mesh in the region where dynamic recrystallization happened as shown in Fig. 18. The black blocks in the figures show the region where DRX happened at the strain of 37.5% when tensile loading is applied in the x direction.

4. Conclusions

In this study, LSMDS was used to characterize the microstructure of Fe–Cr–Ni SS directionally solidified from the liquid state. In order to understand the uniformity in mechanical properties, uniaxial tensile test were performed from x and z directions. The following conclusions were drawn from the simulation results:

Manuscript version: Accepted 19 February 2021
Elsevier, Materials Science & Engineering
https://doi.org/10.1016/j.msea.2021.140999

1.Directional solidification caused the formation of polycrystal structure including HAGBs, thermal twins and DL dissociation (SFs) with a non-uniform dispersion of DLs.

2.A higher level of UTS was observed from x direction (solidification direction) due to a higher interaction of DLs with TBs and GBs.

3.A gradient strain and back stress strengthening were observed in such TWIP steels mainly due to the presence of thermal and mechanical TBs.

4.Significant activity of DLs (planar slip) in multi slip systems as well as mechanical TBs and their interaction with themselves and GBs were observed during deformation.

5.Secondary and ternary TBs were nucleated by interaction of DLs (SFs) with each other and with TBs. Different strengthening and softening mechanisms during microstructural evolution were shown and proposed.

6.The formation of new grains due to migration of GBs and dynamic recrystallization was observed and discussed in detail.

Acknowledgments

Special thanks should be given to The Irish Centre for High-End Computing (ICHEC) for providing required facilities and high-performance computers. We are also grateful to Dr. Akbar Heidarzadeh for assistance with scientific discussion of the results.

This publication has emanated from research supported in part by a grant from Science Foundation Ireland under Grant number 16/RC/3872. For the purpose of Open Access, the author has applied a CC BY public copyright licence to any Author Accepted Manuscript version arising from this submission.

References

I. Gibson, D.W. Rosen, B. Stucker, et al.Additive Manufacturing Technologies, vol. 17, Springer (2014)

[2] M. Gündüz, E. Çadırlı, Directional solidification of aluminium–copper alloys, Mater. Sci. Eng., A, 327 (2) (2002), pp. 167-185, 10.1016/S0921-5093(01)01649-5

[3] M. H. Grabow, G. H. Gilmer, A. F. Bakker, Molecular dynamics studies of silicon solidification and melting, MRS Online Proceedings Library Archive 141. doi:10.1557/PROC-141-349.

[4] M. Bahramyan, R.T. Mousavian, D. Brabazon, Determination of atomic-scale structure and compressive behavior of solidified alxcrcofecuni high entropy alloys, Int. J. Mech. Sci., 171 (2020), p. 105389, 10.1016/j.ijmecsci.2019.105389

[5] M. Bahramyan, R.T. Mousavian, D. Brabazon, Study of the plastic deformation mechanism of trip–twip high entropy alloys at the atomic level Int. J. Plast., 127 (2020), p. 102649, 10.1016/j.ijplas.2019.102649

[6] D.C. Rapaport, D.C.R. Rapaport, The Art of Molecular Dynamics Simulation, Cambridge university press (2004)

[7] E. Asadi, M.A. Zaeem, S. Nouranian, M.I. Baskes, Two-phase solid–liquid coexistence of ni, cu, and al by molecular dynamics simulations using the modified embedded-atom method, Acta Mater., 86 (2015), pp. 169-181, 10.1016/j.actamat.2014.12.010

[8] A. Mahata, M.A. Zaeem, Effects of solidification defects on nanoscale mechanical properties of rapid directionally solidified al-cu alloy: a large scale molecular dynamics study, J. Cryst. Growth, 527 (2019), p. 125255, 10.1016/j.jcrysgro.2019.125255

[9] N.T. Brown, E. Martinez, J. Qu, Interfacial free energy and stiffness of aluminum during rapid solidification, Acta Mater., 129 (2017), pp. 83-90, 10.1016/j.actamat.2017.02.033

[10] D. Zhang, S. Chaudhuri, Solidification dynamics and microstructure evolution in nanocrystalline cobalt, Comput. Mater. Sci., 160 (2019), pp. 222-232, 10.1016/j.commatsci.2018.10.008

[11] Z. Zhao, J. Liu, A.K. Soh, C. Tang, Temperature-mediated fabrication, stress-induced crystallization and transformation: atomistic simulations of additively manufactured amorphous cu pillars, Model. Simulat. Mater. Sci. Eng., 27 (7) (2019), Article 075012, 10.1088/1361-651X/ab3758

[12] J. Nandy, N. Yedla, P. Gupta, H. Sarangi, S. Sahoo,Sintering of alsi10mg particles in direct metal laser sintering process: a molecular dynamics simulation study, Mater. Chem. Phys., 236 (2019), p. 121803, 10.1016/j.matchemphys.2019.121803

[13] J. Zhang, Y. Zhang, W.H. Lee, L. Wu, H.-H. Choi, Y.-G. Jung, A multi-scale multi-physics modeling framework of laser powder bed fusion additive manufacturing process, Met. Powder Rep., 73 (3) (2018), pp. 151-157, 10.1016/j.mprp.2018.01.003

[14] F. Rahmani, J. Jeon, S. Jiang, S. Nouranian, Melting and solidification behavior of cu/al and ti/al bimetallic core/shell nanoparticles during additive manufacturing by molecular dynamics simulation, J. Nanoparticle Res., 20 (5) (2018), p. 133, 10.1007/s11051-018-4237-z

[15] J. Nandy, S. Sahoo, N. Yedla, H. Sarangi, Molecular dynamics simulation of coalescence kinetics and neck growth in laser additive manufacturing of aluminum alloy nanoparticles, J. Mol. Model. 26 (6). doi:10.1007/s00894-020-04395-4.

[16] S. Kurian, R. Mirzaeifar, Selective laser melting of aluminum nano-powder particles, a molecular dynamics study, Additive Manufacturing (2020), p. 101272, 10.1016/j.addma.2020.101272

[17] Q. Jiang, H. Liu, J. Li, D. Yang, Y. Zhang, W. Yang, Atomic-level understanding of crystallization in the selective laser melting of fe50ni50 amorphous alloy, Additive Manufacturing (2020), p. 101369, 10.1016/j.addma.2020.101369

[18] S. Karewar, J. Sietsma, M. Santofimia, Effect of pre-existing defects in the parent fcc phase on atomistic mechanisms during the martensitic transformation in pure fe: a molecular dynamics study, Acta Mater., 142 (2018), pp. 71-81, 10.1016/j.actamat.2017.09.049

[19] X. Zhao, C. Lu, A.K. Tieu, L. Zhan, M. Huang, L. Su, L. Pei, L. Zhang, Deformation twinning and dislocation processes in nanotwinned copper by molecular dynamics simulations, Comput. Mater. Sci., 142 (2018), pp. 59-71, 10.1016/j.commatsci.2017.09.055

[20] J. Ding, H.-n. Zhao, L.-s. Wang, X. Huang, J. Wang, K. Song, S.-q. Lu, X.-g. Zeng, Influence of loading directions on dislocation slip mechanism of nanotwinned ni with void defect at the twin boundary, Comput. Mater. Sci., 152 (2018), pp. 1-11, 10.1016/j.commatsci.2018.05.026

[21] S. Yan, Q.-H. Qin, Z. Zhong, On the real-time atomistic deformation of nano twinned crcofeni high entropy alloy, Nanotechnologydoi:10.1088/1361-6528/ab99ef.

[22] R. Mohammadzadeh, M. Mohammadzadeh, Inverse grain size effect on twinning in nanocrystalline twip steel, Mater. Sci. Eng., A, 747 (2019), pp. 265-275, 10.1016/j.msea.2018.11.085

[23] R. Mohammadzadeh, Reversible deformation in nanocrystalline twip steel during cyclic loading by partial slip reversal and detwinning, Mater. Sci. Eng., A (2020), p. 139251, 10.1016/j.msea.2020.139251

[24] P. Wang, S. Xu, J. Liu, X. Li, Y. Wei, H. Wang, H. Gao, W. Yang, Atomistic simulation for deforming complex alloys with application toward twip steel and associated physical insights, J. Mech. Phys. Solid., 98 (2017), pp. 290-308, 10.1016/j.jmps.2016.09.008

[25] X.W. Zhou, M.E. Foster, R.B. Sills, An fe-ni-cr embedded atom method potential for austenitic and ferritic systems, J. Comput. Chem., 39 (29) (2018), pp. 2420-2431, 10.1002/jcc.25573

[26] S. Plimpton, Fast parallel algorithms for short-range molecular dynamics, J. Comput. Phys., 117 (1) (1995), pp. 1-19, 10.1006/jcph.1995.1039

[27] A. Stukowski, Visualization and analysis of atomistic simulation data with ovito–the open visualization tool, Model. Simulat. Mater. Sci. Eng., 18 (1) (2009), Article 015012, 10.1088/0965-0393/18/1/015012

[28] D. Faken, H. Jónsson, Systematic analysis of local atomic structure combined with 3D computer graphics, Comput. Mater. Sci., 2 (2) (1994), pp. 279-286, 10.1016/0927-0256(94)90109-0

[29] H. Tsuzuki, P.S. Branicio, J.P. Rino, Structural characterization of deformed crystals by analysis of common atomic neighbourhood, Comput. Phys. Commun., 177 (6) (2007), pp. 518-523, 10.1016/j.cpc.2007.05.018

[30] A. Stukowski, V.V. Bulatov, A. Arsenlis, Automated identification and indexing of dislocations in crystal interfaces, Model. Simulat. Mater. Sci. Eng., 20 (8) (2012), Article 085007, 10.1088/0965-0393/20/8/085007

[31] Y.M. Wang, T. Voisin, J.T. McKeown, J. Ye, N.P. Calta, Z. Li, Z. Zeng, Y. Zhang, W. Chen, T.T. Roehling, et al., Additively manufactured hierarchical stainless steels with high strength and ductility, Nat. Mater., 17 (1) (2018), pp. 63-71, 10.1038/NMAT5021

[32] L. Liu, Q. Ding, Y. Zhong, J. Zou, J. Wu, Y.-L. Chiu, J. Li, Z. Zhang, Q. Yu, Z. Shen, Dislocation network in additive manufactured steel breaks strength–ductility trade-off, Mater. Today, 21 (4) (2018), pp. 354-361, 10.1016/j.mattod.2017.11.004

[33] E. Polatidis, J. Čapek, A. Arabi-Hashemi, C. Leinenbach, M. Strobl, High ductility and transformation-induced-plasticity in metastable stainless steel processed by selective laser melting with low power, Scripta Mater., 176 (2020), pp. 53-57, 10.1016/j.scriptamat.2019.09.035

[34] F. Yuan, W. Cheng, S. Zhang, X. Liu, X. Wu, Atomistic simulations of tensile deformation in a crconi medium-entropy alloy with heterogeneous grain structures, Materialia, 9 (2020), p. 100565, 10.1016/j.mtla.2019.100565

[35] Y. Tian, J. Ding, X. Huang, H.-r. Zheng, K. Song, S.-q. Lu, X.-g. Zeng, Plastic deformation mechanisms of tension-compression asymmetry of nano-polycrystalline tial: twin boundary spacing and temperature effect, Comput. Mater. Sci., 171 (2020), p. 109218, 10.1016/j.commatsci.2019.109218

[36] J. Sun, H. Ye, J. Tao, Q. Li, J. Zhang, L. Shen, Y. Zheng, H. Zhang, Gradient structure regulated plastic deformation mechanisms in polycrystalline nanotwinned copper, J. Phys. Appl. Phys., 52 (36) (2019), p. 365304, 10.1088/1361-6463/ab29ca

[37] M. Zhang, K. Sun, L. Fang, Influence of grain boundary activites on elastic and plastic deformation of nanocrystalline cu as studied by phase filed and atomistic simulation, Int. J. Mech. Sci. (2020), p. 105911, 10.1016/j.ijmecsci.2020.105911

[38] Z. Yan, Y. Lin, Lomer-cottrell locks with multiple stair-rod dislocations in a nanostructured al alloy processed by severe plastic deformation, Mater. Sci. Eng., A, 747 (2019), pp. 177-184, 10.1016/j.msea.2019.01.066

[39] D. Choudhuri, B. Gwalani, S. Gorsse, M. Komarasamy, S.A. Mantri, S.G. Srinivasan, R.S. Mishra, R. Banerjee, Enhancing strength and strain hardenability via deformation twinning in fcc-based high entropy alloys reinforced with intermetallic compounds, Acta Mater., 165 (2019), pp. 420-430, 10.1016/j.actamat.2018.12.010

[40] H. Zhi, S. Antonov, C. Zhang, Z. Guo, Y. Su, Origins of back stress strengthening in fe-22mn-0.6 c (-3al) twip steels, Mater. Sci. Eng., A (2020), p. 139834, 10.1016/j.msea.2020.139834

[41] R. Su, D. Neffati, S. Xue, Q. Li, Z. Fan, Y. Liu, H. Wang, Y. Kulkarni, X. Zhang, Deformation mechanisms in fcc co dominated by high-density stacking faults, Mater. Sci. Eng., A, 736 (2018), pp. 12-21, 10.1016/j.msea.2018.08.057

[42] Q. Fang, F. Sansoz, Influence of intrinsic kink-like defects on screw dislocation–coherent twin boundary interactions in copper, Acta Mater., 123 (2017), pp. 383-393, 10.1016/j.actamat.2016.10.032

[43] X. Hu, Y. Ni, Z. Zhang, Atomistic study of interactions between intrinsic kink defects and dislocations in twin boundaries of nanotwinned copper during nanoindentation, Nanomaterials, 10 (2) (2020), p. 221, 10.3390/nano10020221

[44] J. Du, Z. Wu, E. Fu, Y. Liang, X. Wang, P. Wang, K. Yu, X. Ding, M. Li, M. Kirk, Detwinning through migration of twin boundaries in nanotwinned cu films under in situ ion irradiation, Sci. Technol. Adv. Mater., 19 (1) (2018), pp. 212-220, 10.1080/14686996.2018.1428877

[45] J. Wang, N. Li, O. Anderoglu, X. Zhang, A. Misra, J. Huang, J. Hirth Detwinning mechanisms for growth twins in face-centered cubic metals Acta Mater., 58 (6) (2010), pp. 2262-2270, 10.1016/j.actamat.2009.12.013

[46] Y. Liang, X. Yang, M. Gong, G. Liu, Q. Liu, J. Wang, Interactions between dislocations and three-dimensional annealing twins in face centered cubic metals, Comput. Mater. Sci., 161 (2019), pp. 371-378, 10.1016/j.commatsci.2019.02.024

[47] Z. Zhang, H. Sheng, Z. Wang, B. Gludovatz, Z. Zhang, E.P. George, Q. Yu, S.X. Mao, R.O. Ritchie, Dislocation mechanisms and 3d twin architectures generate exceptional strength-ductility-toughness combination in crconi medium-entropy alloy, Nat. Commun., 8 (1) (2017), pp. 1-8, 10.1038/ncomms14390

[48] X. Zhao, C. Lu, A.K. Tieu, L. Pei, L. Zhang, L. Su, L. Zhan, Deformation mechanisms in nanotwinned copper by molecular dynamics simulation, Mater. Sci. Eng., A, 687 (2017), pp. 343-351, 10.1016/j.msea.2016.12.061

[49] A. Rajput, S.K. Paul, Effect of different tensile loading modes on deformation behavior of nanocrystalline copper: atomistic simulations, Results in Materials, 4 (2019), p. 100042, 10.1016/j.rinma.2019.100042

[50] J.B. Jeon, G. Dehm, Formation of dislocation networks in a coherent cu σ3 (1 1 1) twin boundary, Scripta Mater., 102 (2015), pp. 71-74, 10.1016/j.scriptamat.2015.02.016

[51] M. Zhang, T. Xu, L. Fang, Grain boundaries dependence of plastic deformation in nanocrystalline cu film investigated by phase field and molecular dynamics methods, Mater. Chem. Phys. (2020), p. 123506, 10.1016/j.matchemphys.2020.123506

[52] Q. Liu, G. Wang, C. Qiu, On the role of dynamic grain movement in deformation and mechanical anisotropy development in a selectively laser melted stainless steel, Additive Manufacturing (2020), p. 101329, 10.1016/j.addma.2020.101329

Manuscript version: Accepted 19 February 2021
Elsevier, Materials Science & Engineering
https://doi.org/10.1016/j.msea.2021.140999

[53] X. Wang, J. Mu iz Lerma, O. Sanchez-Mata, M.A. Shandiz, N. Brodusch, R. Gauvin, M. Brochu, Characterization of single crystalline austenitic stainless steel thin struts processed by laser powder bed fusion, Scripta Mater., 163 (2019), pp. 51-56, 10.1016/j.scriptamat.2018.12.032